

## *Styles of underplating in the Marin Headlands terrane, Franciscan complex, California*

**Christine A. Regalla**

*Department of Earth and Environment, Boston University, 685 Commonwealth Avenue, Boston, Massachusetts 02215, USA*

**Christie D. Rowe**

**Nicolas Harrichhausen\***

**Matthew S. Tarling<sup>†</sup>**

**Jyotsana Singh**

*Earth & Planetary Sciences Department, McGill University, 3450 University Street, Montréal, Québec H3A 0E8, Canada*

### ABSTRACT

Geophysical images and structural cross sections of accretionary wedges are usually aligned orthogonal to the subduction trench axis. These sections often reveal underplated duplexes of subducted oceanic sediment and igneous crust that record trench-normal shortening and wedge thickening facilitated by down-stepping of the décollement. However, this approach may underrecognize trench-parallel strain and the effects of faulting associated with flexure of the downgoing plate. New mapping of a recently exposed transect across a portion of the Marin Headlands terrane, California, United States, documents evidence for structural complexity over short spatio-temporal scales within an underplated system. We documented the geometry, kinematics, vergence, and internal architecture of faults and folds along ~2.5 km of section, and we identified six previously unmapped intraformational imbricate thrusts and 13 high-angle faults that accommodate shortening and flattening of the underthrust section. Thrust faults occur within nearly every lithology without clear preference for any stratigraphic horizon, and fold vergence varies between imbricate sheets by ~10°–40°. In our map area, imbricate bounding thrusts have relatively narrow damage zones (≤5–10 m) and sharp, discrete fault cores and lack veining, in contrast to the wide, highly veined fault zones previously documented in the Marin Headlands terrane. The spacing of imbricate thrusts, combined with paleoconvergence rates, indicates relatively rapid generation of new fault surfaces on ~10–100 k.y. time scales, a process that may contribute to strain hardening and locking within the seismogenic zone. The structural and kinematic complexity documented in the Marin Headlands is an example of the short spatial and temporal scales of heterogeneity that may characterize regions of active underplating. Such features are smaller than the

\*Current address: Department of Earth Science, University of California, Santa Barbara, California 93106, USA.

<sup>†</sup>Current address: Department of Geology, University of Otago, P.O. Box 56, Dunedin 9054, New Zealand.

Regalla, C.A., Rowe, C.D., Harrichhausen, N., Tarling, M.S., and Singh, J., 2018, Styles of underplating in the Marin Headlands terrane, Franciscan complex, California, *in* Byrne, T., Underwood, M.B., Fisher, D., McNeill, L., Saffer, D., Ujiie, K., and Yamaguchi, A., eds., *Geology and Tectonics of Subduction Zones: A Tribute to Gaku Kimura*: Geological Society of America Special Paper 534, p. , [https://doi.org/10.1130/2018.2534\(10\)](https://doi.org/10.1130/2018.2534(10)).

© 2018 The Geological Society of America. All rights reserved. For permission to copy, contact [editing@geosociety.org](mailto:editing@geosociety.org).

**typical spatial resolution of geophysical data from active subduction thrusts and may not be readily resolved, thus highlighting the need for cross-comparison of geophysical data with field analogues when evaluating the kinematic and mechanical processes of underplating.**

## INTRODUCTION

Underplating is a ubiquitous process in subduction zone forearcs that contributes to mass transfer from the lower plate to the upper plate through the down-stepping of the plate-boundary interface into underthrust sediment and uppermost igneous crust. Underplating typically occurs at depths of ~5–20 km and temperatures of ~250–300 °C (e.g., Rowe et al., 2013), at conditions where basalt, graywacke, and pelagic sediments of the down-going slab undergo low-grade metamorphism, alteration, and diagenesis during tectonic burial and subduction-related shearing (e.g., Sample and Fisher, 1986; Kimura and Mukai, 1991; Moore et al., 2007). The accompanying changes in the rheologic properties of the subducting plate control the strength and mechanics of the plate interface (Moore and Saffer, 2001).

Down-stepping of the plate boundary is ultimately the combined result of strengthening and strain hardening of the original plate-boundary thrust and weakening of rocks in the underthrust section, particularly in hydrated basaltic crust. The temperature range associated with underplating corresponds to the mid- to lower seismogenic zone in subduction plate boundaries (Moore et al., 2007) and to regions of the plate interface that are geotectonically locked in many modern margins (e.g., Hyndman et al., 1995; Oleskevich et al., 1999). Thus, the strain hardening processes that promote underplating may be a direct record of locking of the subduction thrust, and the mechanics of underplated packages may play a role in the accumulation of interseismic strain and nucleation of megathrust earthquakes.

Underplating along active margins has been inferred from multichannel seismic lines and relocations of repeating micro-earthquakes (Moore et al., 1991; Calvert, 2004; Kimura et al., 2010; St. Clair et al., 2016). Networks of dipping reflectors and low-velocity zones at 10–20 km depth along the Cascadia, Aleutian, southern Japan, and Costa Rican margins have been interpreted to be reflected underplated sheets ~15–40 km long and ~1–3.5 km thick (Moore et al., 1991; Calvert, 2004; Kimura et al., 2010; St. Clair et al., 2016). However, imbricate sheets in fault duplexes documented in exhumed terranes have fault spacing of 0.5 km or less in the dip direction and may be laterally continuous for only ~1–5 km (Kimura et al., 1992, 1996; Hashimoto and Kimura, 1999; Onishi et al., 2001). These scales are below the typical resolution of geophysical methods at these depths. Interpretation of the four-dimensional evolution of underplated structures in modern settings, therefore, requires comparison to analogue fault systems exposed in outcrops of ancient accreted terranes.

In this contribution, we document the structural complexity of fault geometry, kinematics, and deformation structures within

underplated units spectacularly exposed in the Mesozoic Marin Headlands terrane of the Franciscan complex, northern California. Here, a 2.5-km-long section of new, nearly continuous outcrop produced by recent road work provides unprecedented exposure of the internal structure of the underplated imbricate sheets of low-grade metabasalt (greenstone), chert, and graywacke along an ~1.5 km dip-perpendicular section. Within these exposures, we mapped numerous, previously undocumented, high-angle faults, identified previously unmapped imbricate thrusts localized in multiple lithologic horizons, documented significant variance in vergence between adjacent fault-bounded packages, and observed a large variety of internal fault architecture. Our observations provide evidence for frequent initiation and abandonment of short fault segments with minimal throw at the 10–100 k.y. time scale within the underplated sequence. This style of deformation may be associated with multistage flattening during underthrusting, deformation with a trench-parallel component of strain, or deformation in association with the subduction of rough seafloor bathymetry. We propose that the structural heterogeneity documented in this portion of the Marin Headlands terrane may serve as a type example of the style of deformational complexity that can be expected in regions where active underplating occurs at modern margins.

## GEOLOGIC BACKGROUND

The Marin Headlands terrane, exposed in the Golden Gate National Recreation Area, Marin County, California, is composed of imbricate sheets of low-grade metabasalt, chert, and turbiditic graywacke (Wahrhaftig, 1984a, 1984b). The distinctive chert and metabasalt lithologic assemblage in the Marin Headlands terrane provides marker beds that allow better delineation of structures than in adjacent graywacke-dominated terranes of the Franciscan complex. The first published map of the Marin Headlands terrane (Wahrhaftig, 1984a; compiled into Marin County map by Graymer et al., 2006) identified  $\geq 10$  imbricate thrust sheets, each ~300–500 m thick in map view, along an ~4-km-long strike-perpendicular section (Wahrhaftig, 1984a). Individual lithologic units within imbricate sheets range from 0 to 300 m thick (Fig. 1; Wahrhaftig, 1984a; Murchey, 1984; Murchey and Jones, 1984), but evidence for substantial internal thickening is demonstrated by extraordinary fold arrays in chert sections (e.g., Wahrhaftig, 1984a, 1984b).

Paleomagnetic rotations in pillow basalts (Curry et al., 1984) and radiolarian microfossil assemblages (Murchey and Jones, 1984) support formation of basaltic crust and deposition of the cherts at an equatorial paleolatitude. Microfossil assemblages indicate the cherts were deposited between the Early Jurassic

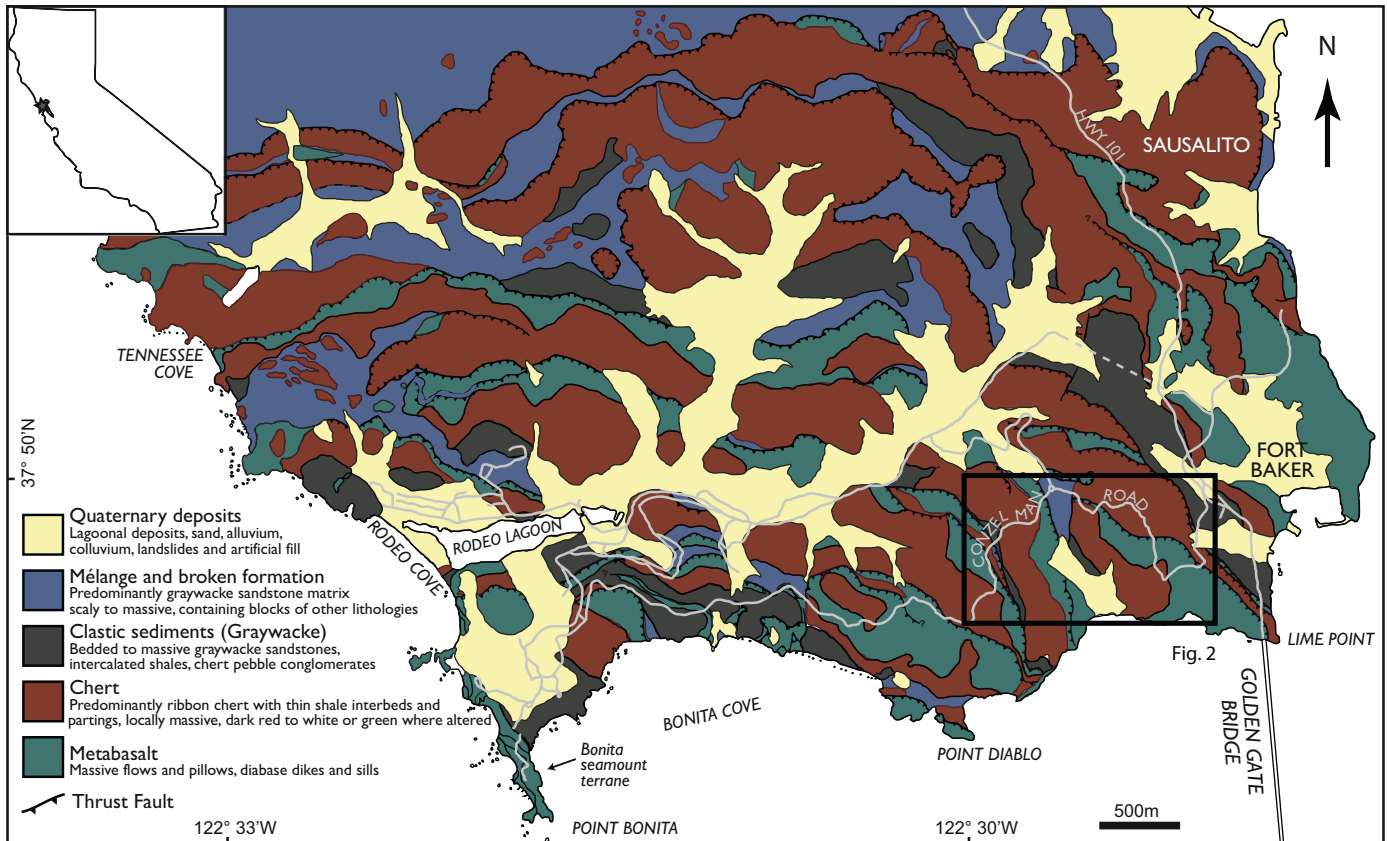


Figure 1. Geologic map of the Marin Headlands terrane, Marin County, California, modified after Wahrhaftig (1984a). Inset shows location of map area, north of San Francisco, California. Box shows area of inset geologic map in Figure 2.

and late Early Cretaceous directly on Lower Jurassic ocean floor pillow basalts with mid-ocean-ridge basalt (MORB)-like trace-element patterns (Karl, 1984; Murchey, 1984; Murchey and Jones, 1984; Wahrhaftig, 1984a; Ghatak et al., 2012). Accretion to North America occurred shortly after deposition of graywackes, shales, and conglomerates on top of the chert sequence during the Cenomanian (Curry et al., 1984). Peak metamorphic conditions recorded in the metabasalts of the Marin Headlands terrane at Rodeo Cove correspond to temperatures between 200 °C and 250 °C at depths of 8–10 km (Meneghini and Moore, 2007), near the middle of the thermally defined seismogenic zone (Moore et al., 2007). Since accretion, the imbricated nappes of the Marin Headlands terrane have been rotated  $130.5^\circ \pm 11.1^\circ$  clockwise around a vertical axis (Curry et al., 1984), and the originally northeast-dipping imbricate thrusts now dip toward the south (Fig. 1). This rotation was likely caused by block rotation within early San Andreas strike-slip fault systems after underplating to the Franciscan accretionary wedge (Curry et al., 1984).

## GEOLOGIC MAPPING AND LITHOLOGIC UNITS

We mapped ~2.5 km of road-cut exposure on Conzelman Road (Fig. 2), which corresponds to ~1.5 km of dip section

through the imbricate structures of the Marin Headlands terrane. The nearly 100% exposure along this road is unequalled in the region and allows direct observation of the imbricate thrusts that bound the major packages, as well as smaller-offset faults that internally deform the packages. We mapped subsidiary structures using a reference stratigraphy modified from Murchey (1984) that consists of greenstone, red chert, white chert, graywacke, and mélangé.

Greenstone occurs at the base of many, but not all, of the thrust fault packages mapped along Conzelman Road. Greenstones consist of dark-green to black pillow basalts (Fig. 3A) and vesicular flows that weather green to brownish red (Fig. 3B). Pillows 30–100 cm in diameter are well preserved in some sections (Fig. 3A), allowing robust measurements of bedding orientation, while other sections are massive, and bedding is ambiguous (Fig. 3B). Near contacts with other lithologies, especially in the vicinity of major faults, the metabasalt is cut by anastomosing networks of fractures. Phacoids of metabasalt within these networks often have striated shiny dark-green to black surfaces, indicating shear along the anastomosing fractures. This fabric is similar to the “scaly fabric” often developed in phyllosilicate-rich rocks, so we designate metabasalts displaying this fabric as “scaly metabasalts” (Fig. 3C). Analysis of bulk mineralogy in scaly metabasalts

*Styles of underplating in the Marin Headlands terrane, Franciscan complex, California*

in thin section and with X-ray diffraction (XRD) confirmed the presence of chlorite (clinochlore), epidote, albite, augite, and trace zeolite (bogsite), and calcite (Fig. 4). Chlorite makes up 40%–50% of the rock, which may explain why it has developed a deformation fabric commonly associated with phyllosilicate-rich rocks such as pelites. We found that the bedding or pillow orientations indicated stratigraphy becomes younger to the southwest (structurally up section), in agreement with Wahrhaftig (1984a). Aside from local short limbs in tight folds, none of the sediments or volcanic units was found to be overturned.

We distinguished two chert subunits based on a simplification of the lithostratigraphic units of Murchey (1984), consisting of an upper “red chert unit,” which is predominantly deep red in color, and a lower “white chert unit,” which varies from

green to white to locally red/ocher. We utilized a simplified scheme because we found that the contacts between the subunits of Murchey (1984) were not sufficiently distinctive or continuous to be a useful stratigraphic marker by which to quantitatively estimate fault offset of the section. The boundaries between red, ocher, and green chert do not always follow bedding; therefore, they probably reflect diagenetic oxidation/reduction horizons or fluid conduits (Figs. 3D and 3E), as documented in the Mino belt of southern Japan (Kameda et al., 2012; Yamaguchi et al., 2106).

In our section, we observed the following lithologic characteristics that we used to infer approximate position within the chert section. The basal contact of chert overlying metabasalt is sheared at all but one location in our map area (S1 in Fig. 2). At this site, chert bedding interfingers with volcanic layers, and a

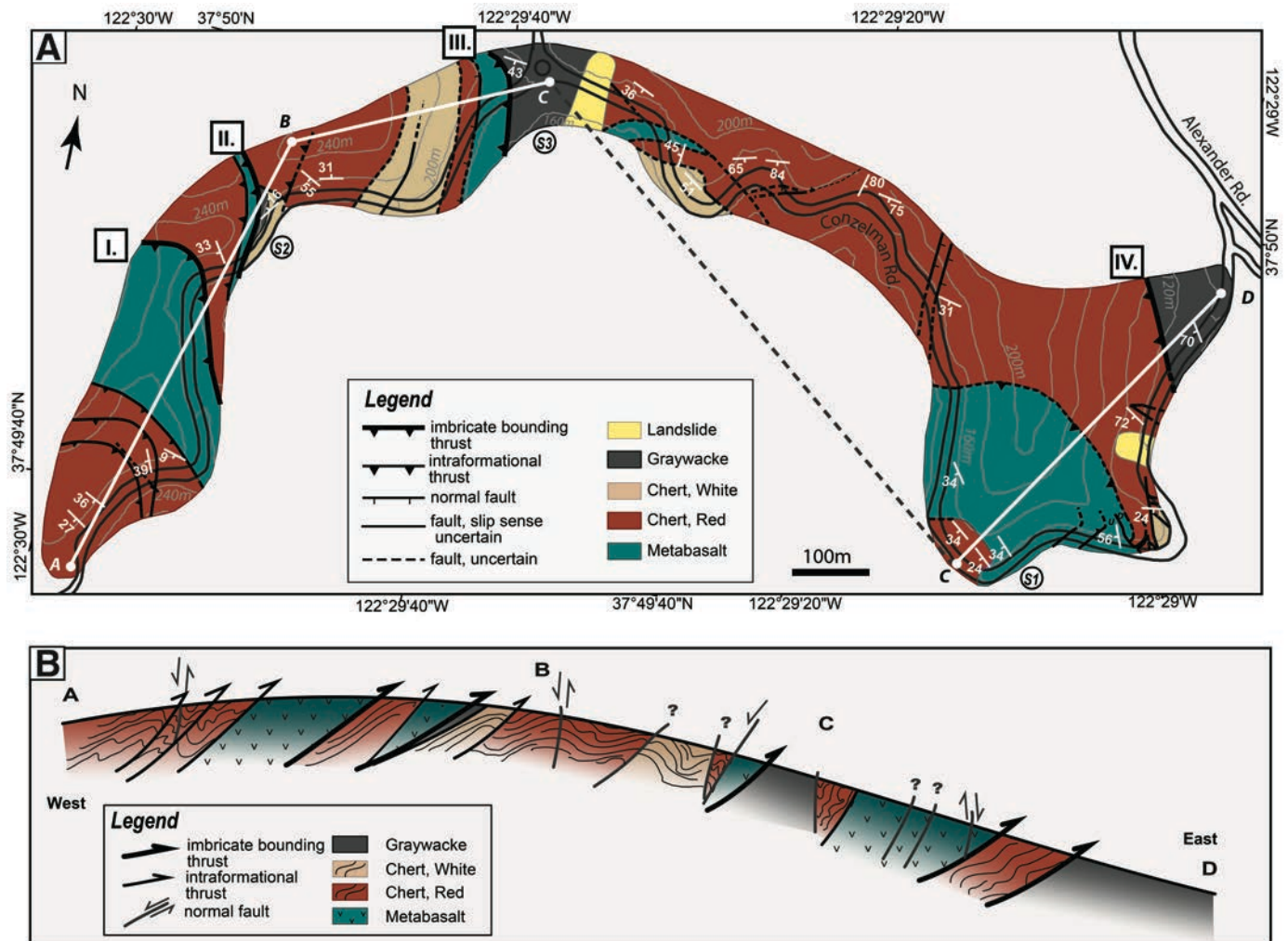


Figure 2. (A) New mapping along Conzelman Road, showing the complexity of deformation in the Marin Headlands terrane. Roman numerals indicate major imbricate bounding thrusts. Line of cross section is indicated along A–B–C–D. (B) Schematic cross section through mapped area in part A, along ~1.5 km of dip section. Linework in chert indicates style of folding within each fault-bounded section.

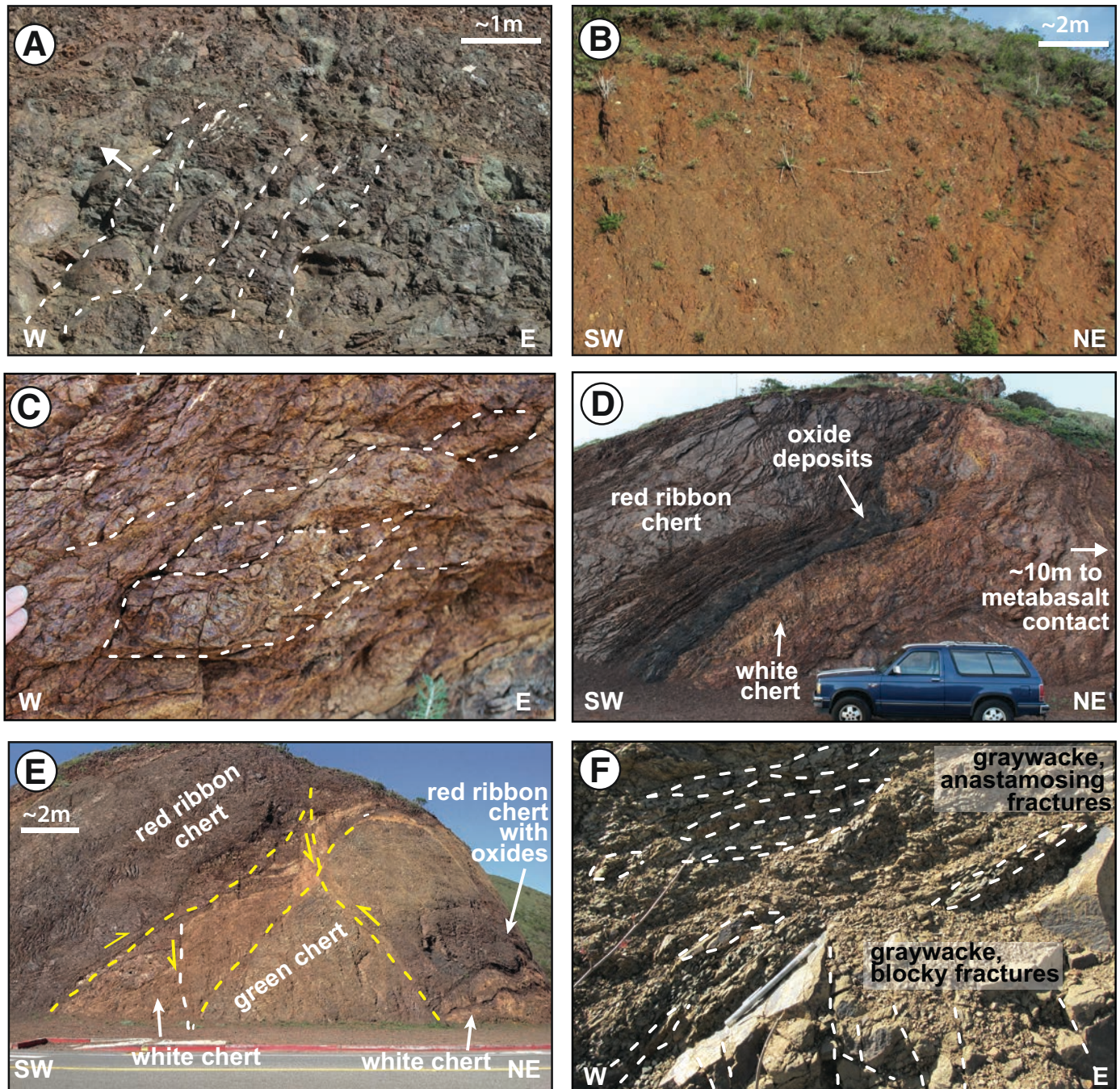


Figure 3. Outcrop appearance of major lithologies of the Marin Headlands terrane. (A) Dark-green basaltic pillows (each bedding layer is ~30–60 cm thick, marked by white dotted lines). Younging direction is indicated with white arrow. (B) Red-weathering metabasalt exposure. (C) Red-weathering sheared metabasalt with scaly fabric in the hanging wall of an imbricate thrust (imbricate fault II). X-ray diffraction (XRD) spectra from this outcrop are shown in Figure 4. (D) Roadcut showing a section of discolored (white) chert in contact with an overlying oxide deposit layer, near the depositional contact with metabasalt. (E) Fault intercalation (yellow dashed lines) of blocks of green and red ribbon cherts. Apparent displacement is indicated with yellow arrows. (F) Exposure of fractured graywacke (footwall of imbricate fault III) showing a lower unit with bedding-orthogonal, blocky fractures, and an upper unit with anastomosing fracture network. White dashed lines trace fractures surrounding relatively coherent blocks. XRD spectra from this outcrop are shown in Figure 4.

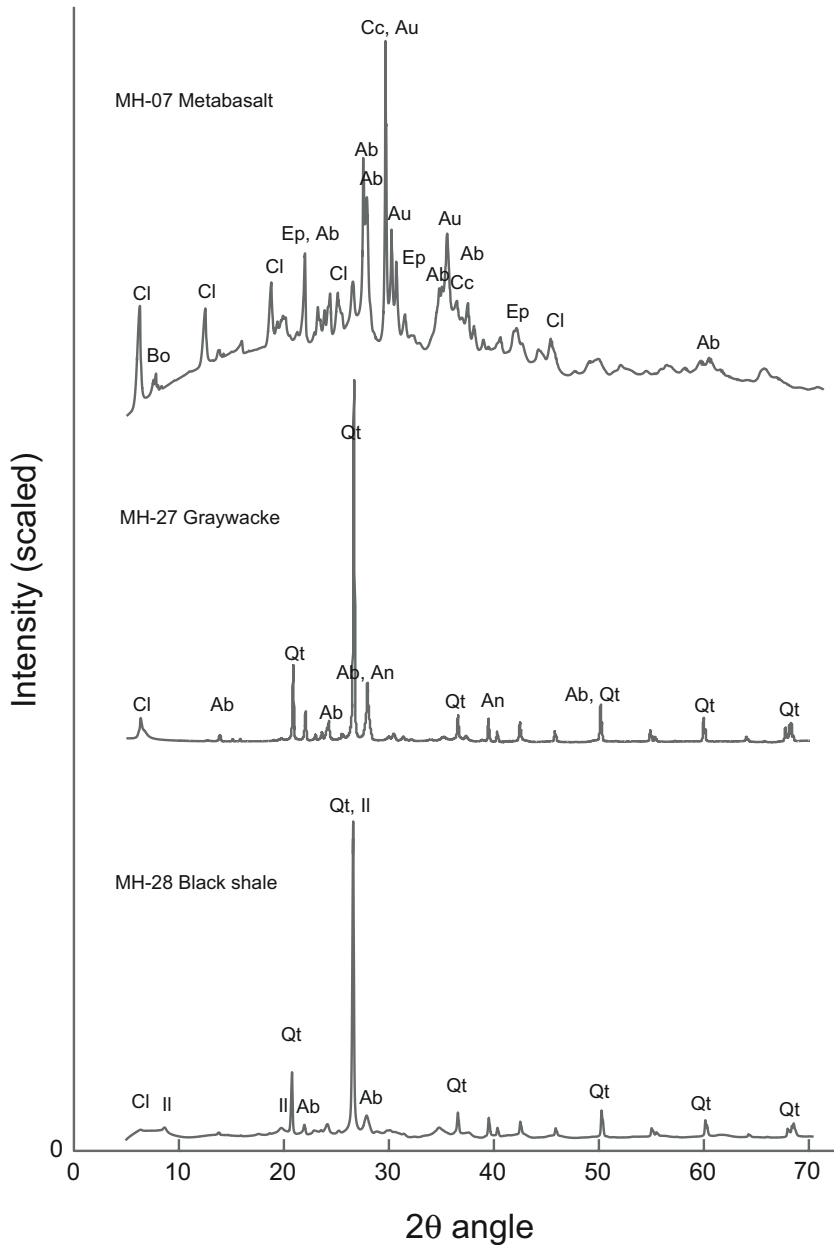


Figure 4. X-ray diffraction (XRD) spectra from metabasalt (sample MH-07), metagraywacke (sample MH-27), and black shale (sample MH-28) located in the hanging wall (metabasalt) and footwall (sediments) of imbricate thrust II. Peaks are labeled by mineral identified. Ab—albite, An—anorthoclase (alkali feldspar), Au—augite, Bo—boggsite (zeolite), Cc—calcite, Cl—chlorite (clinochlore), Ep—epidote, Il—illite, Qt—quartz.

laminated bed of black, oxide-rich sediment lies just above the interfingered contact, confirming the conformability of the layers. Both chert and volcanic rocks are intensely altered and are light-green/white at the depositional contact (Figs. 3D and 3E). The observation of white-green chert along the clearly altered depositional contact confirms that the chert color cannot be correlated uniquely to stratigraphic position, as was reported by Murchey (1984). The lowermost 10–15 m section displays massive bedding with abundant lenses of quartz-cemented breccia and black metallic oxide staining and may be red, green, or white (Figs. 3D and 3E). This section is overlain by a thicker sequence (~30–50 m) of homogeneous, thin-bedded brick-red ribbon cherts with red shale partings, which form the middle of the sec-

tion (Fig. 3D). The upper approximate third of the section shows more variation in bedding thickness, and white to green alteration is frequently observed. Minor, bedding-normal quartz veins are prevalent, although not ubiquitous in the red ribbon cherts. Veins are beige to white in color, ~0.5–3 mm wide, and occur with a spacing as small as <0.25–1 cm. Where veins are found in folded chert sections, the vein geometry remains orthogonal to bedding around the hinge of the fold, suggesting that the veins predate folding.

The cherts are depositionally overlain by Cenomanian or younger lithic graywackes grading to dark-gray to black shales, interpreted as deep-sea trench turbidites (Wahrhaftig, 1984a, 1984b; Fig. 3F). We observed a conformable sandstone-over-

chert contact at one location on our transect, in the footwall of imbricate fault II (S2 in Fig. 2), where the thin-bedded chert graded into black shale, which transitioned to interbedded graywacke and shale. Sandstones contain angular to subangular clasts of quartz, feldspar, and volcanic fragments in a tan to dark silty matrix visible in hand sample (Wahrhaftig, 1984a). Analysis of bulk mineralogy in graywacke in thin section and by XRD confirms the presence of quartz, albite, alkali feldspar (anorthoclase), and chlorite (clinocllore). Pyrite is also present, but the percentage is too low to detect by bulk XRD (Fig. 4). Black shale contains quartz, illite, chlorite (clinocllore), and albite (Fig. 4). The siltstones and shales are dark gray to black and normally form fining-upward Bouma sequences on top of coarser graywackes. Most of the clastic sediments in our mapped section are coarse to fine sandstones, with rare outcrops of dark-gray shales.

The Marin Headlands terrane imbricate sequence is overthrust on Franciscan *mélange*, and fault-bounded packages of *mélange* and broken sandstone-shale formation are intercalated within the imbricate thrust package (Wahrhaftig, 1984a). *Mélange* in the Marin Headlands terrane consists of a sheared sandstone and shale matrix that may include blocks of sandstone, metabasalt, gabbro, and chert (Wahrhaftig, 1984a, 1984b), which is mimicked closely in appearance by modern landslide deposits, complicating the mapping efforts on hillslopes. Wahrhaftig (1984a) noted that groundwater seeps were common in *mélange* terrane, which may indicate that some of these localities were indeed landslides or earthflows (e.g., Kelsey, 1978). A previously mapped belt of *mélange* that crosses our transect was revealed in the fresh roadcuts to instead be massive, coherently bedded sandstone (cf. Fig. 1 and Fig. 2A, site S3 at traffic circle on Conzelman Road), suggesting that the prevalence of *mélange* in the Marin Headlands terrane may be less than previously mapped (cf. Wahrhaftig, 1984a).

## DEFORMATION STRUCTURES IN THE MARIN HEADLANDS TERRANE

### Fault Geometry and Kinematics

The faults cropping out along Conzelman Road mostly fall into two categories: shallowly to steeply dipping thrust/reverse faults with clear sense of relative motion, and steep faults with variable or undetermined sense of motion. Faults were identified by juxtaposition of different lithologies along a sheared contact, juxtaposition of similar rocks of distinctly different orientation along a sheared contact, and/or evidence of drag/deformation of wall rock, indicating relative motion along a surface. Although the color of chert does not uniquely identify the stratigraphic level within the section, we used sharp color changes across sheared surfaces as indicators of intraformational faults. These identifications were supported by other observations, including sharp changes in bedding style or thickness, changes in orientation of bedding, and/or changes in size, style, and orientation of folds (Figs. 5A–5D).

The positions of major lithologic contacts in our mapping agree well with the regional map by Wahrhaftig (1984a), who identified anastomosing sets of subparallel approximately ESE–WNW–striking, SSW-dipping thrust faults bounding tectonic slivers composing the Marin Headlands terrane. However, while previous mapping identified ~10 major thrusts in an ~3 km dip-parallel transect, each on the order of hundreds of meters of stratigraphic throw, our mapping in an ~1.5 km dip-parallel transect along freshly exposed outcrops on Conzelman Road revealed about twice that density of minor thrust faults, each on the order of tens of meters to ~100 m of stratigraphic throw. We found that the spacing of thrusts in the Marin Headlands terrane is not constant but ranges from a few meters to hundreds of meters (Wahrhaftig, 1984a; this study). Both our mapping and that of Wahrhaftig (1984a) indicate that the along-strike continuity of individual thrust slices is extremely limited. While a few slices within the Marin Headlands terrane have strike lengths on the order of ~2 km extent, most are laterally pinched off by intersections with other thrust faults in less than 1 km of strike distance (Wahrhaftig, 1984a). Last, while Wahrhaftig (1984a) mapped nearly all contacts of chert-over-metabasalt and graywacke-over-chert as depositional, the new outcrop exposures along Conzelman Rd reveal that nearly all lithologic contacts also acted as shear planes.

We mapped 11 thrust faults within the 1.5 km of dip section along Conzelman Road (Fig. 2), including six newly identified, previously unmapped, thrust faults. The existence of these additional faults was predicted by Wahrhaftig (1984a) to explain thickness variations in the chert slices. We documented imbricate thrusts at nearly every stratigraphic level within the underplated sections in the Marin Headlands terrane, and we found faults that duplicate sections within the red chert and within metabasalt, as well as at the metabasalt-chert contact. Our observations suggest that no single lithologic horizon preferentially acted to localize plate-boundary shear, but that new faults were generated in multiple horizons within the basaltic crust and the overlying sediment section.

Thrust faults cutting chert and metabasalt often have thick (~5–20 cm), pinch-and-swell fault cores of brecciated wall rock and gouge and anastomosing slip surfaces, with no drag folds in the surrounding sediments (e.g., Figs. 5E–5F and 6A–6B). Thrust faults cutting graywacke have thinner fault cores (~2–4 mm), and distributed subsidiary faults through the wall rock accommodate some of the fault-parallel slip (Figs. 6F–6G). Thrust faults juxtaposing chert and metabasalt have thin (~10 cm) gouge layers with sharp edges, with 5–10 m of scaly fabric developed in both the hanging wall and footwall (Figs. 5F and 6B). We often observed color alteration of the footwall of a reverse fault in either chert or metabasalt, but without evidence of asymmetry in damage zone fracture density across the fault. We observed several instances where chert bedding in the hanging wall and footwall of a thrust fault was parallel to a fault surface containing gouge or foliated breccia layers. No fault-parallel veins were observed in these fault cores or in the wall rock. In addition, no veins occurred in the fractured damage zones or scaly fabric around the fault cores.

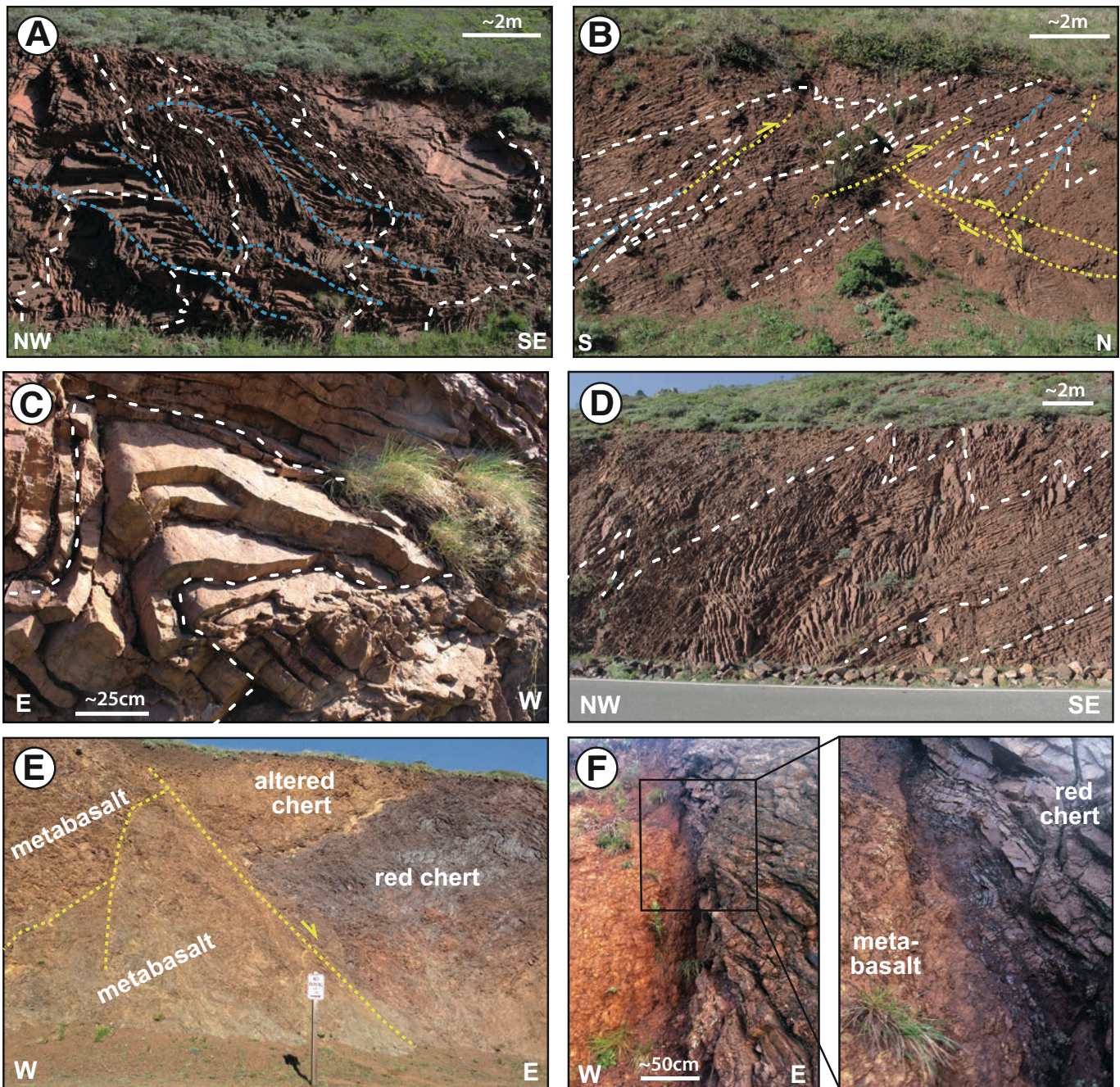


Figure 5. Examples of intraformational deformation in chert. (A) Chaotically folded section of ribbon chert. Selected bedding layers are outlined (white dashed line) to emphasize disharmony in fold sets. Traces (blue dotted line) reveal similarly oriented, nonplanar axial surfaces. Fold asymmetry consistently indicates predominant, but not uniform, northward vergence. (B) Folds in more coherent section of ribbon cherts. White dashed lines outline single bedding planes to reveal fold structure. Folds have sharp hinges and planar limbs with interlimb angle  $\sim 10^{\circ}$ – $50^{\circ}$ , and parallel axial planes. Folds have consistent asymmetry indicating north vergence. Yellow dashed lines show traces of faults. Normal faults that offset folded beds (lower right) are themselves offset by limb-parallel thrust-sense slip along bedding planes (center), suggesting that faulting was contemporaneous with folding. In some cases, fold axial surfaces transition into faults and back to axial surfaces (compare yellow and blue dashed lines). (C) Example of tight, noncylindrical fold with rounded hinge and straight limbs in red ribbon cherts. White lines trace individual bedding planes, showing nonparallel traces. (D) Roadcut showing asymmetric chevron folds in relatively coherent section of ribbon cherts. White lines trace individual bedding planes. Folds are disharmonic but are broadly parallel and consistent in small sections. (E) Example of a high-angle fault with apparent normal displacement, juxtaposing metabasalt and chert. Fault planes are marked by yellow dashed lines. (F) Example of the brecciated fault core of a high-angle fault, with uncertain slip sense, that juxtaposes metabasalt and red chert. (Photo provided by E.M. Rowe.)

Subvertical faults are common throughout the mapped section (Figs. 5E–5F and 7), and we identified 13 new high-angle faults (average spacing in map view ~115 m; Fig. 2) that have not been reported in previous mapping, or that had been mapped as low-angle thrust faults parallel to imbricate thrusts (Wahrhaftig, 1984a). These faults mostly occur as either N–S–striking or E–W–striking sets, in contrast to imbricate thrusts, which tend to strike WNW–ESE (Fig. 7). In contrast to thrust faults, many of the subvertical faults are accompanied by drag folding of the sedimentary layers on one or both sides of the fault. Alteration haloes up to 10–15 cm wide occur in the footwall of some of the faults. These steep faults often occur in isolation, but they are sometimes in sets with mutually crosscutting relationships with bedding-parallel thrust faults (Figs. 3E and 5E–5F).

The majority of mapped high-angle faults have normal sense of slip, but for many faults, we could not determine the sense of apparent offset because no correlatable features or flanking structures were observed within the limits of the outcrop. While it is possible that some of the faults without identified motion indicators are strike-slip faults, we saw no reconstructable dextral offset of depositional or thrust contacts in the Marin Headlands terrane on the map scale (e.g., Fig. 1; Wahrhaftig, 1984a). The possible strike-slip faults we did map cannot be traced across where our strip map should intersect their projections. Therefore, we interpret these as having limited strike length (<~100 m) and only minor strike-slip offset (tens of meters or less), which have minimal effect on the outcrop pattern.

### Internal Structure of Major Imbricate-Bounding Thrust Faults

Two gently-dipping metabasalt-over-graywacke imbricate bounding thrusts, faults II and III (Fig. 6), are spectacularly exposed along Conzelman Road (Fig. 2). Given that the estimated stratigraphic separation on these faults, which cut out the entire chert unit, is at minimum ~90 m, they have each accommodated at least ~0.5–2 km of plate-boundary slip.

Imbricate fault II is an ~4.5-m-thick zone consisting of fault-parallel scaly fabric in metabasalt in the hanging wall, a thin sharp fault core, and scaly fabric developed in graywacke in the footwall (Figs. 2 and 6A–6E). The hanging wall contains ~0.75 m of scaly fabric developed within metabasalt, with an anastomosing foliation that defines ~5 cm by 15–30 cm metabasalt phacoids (Fig. 3C), and grades up section into undeformed metabasalt (Fig. 6A). The scaly metabasalt is in sharp contact with the fault core, and we observed no lithologic mixing across the fault (Figs. 6A–6D). The fault core has an upper ~0.5-cm-wide zone of moderately cohesive medium-gray gouge containing ~0.5–4 mm clasts (Fig. 6D). Below the gray gouge, there is an ~2-mm-wide, black, clayey gouge with a fabric alignment parallel to the contacts of the gouge zone (Fig. 6D). Both the upper and lower contacts of the thin black clay gouge are sharp and planar, and the upper contact is defined by a continuous, discrete principal slip surface that is traceable across the visible

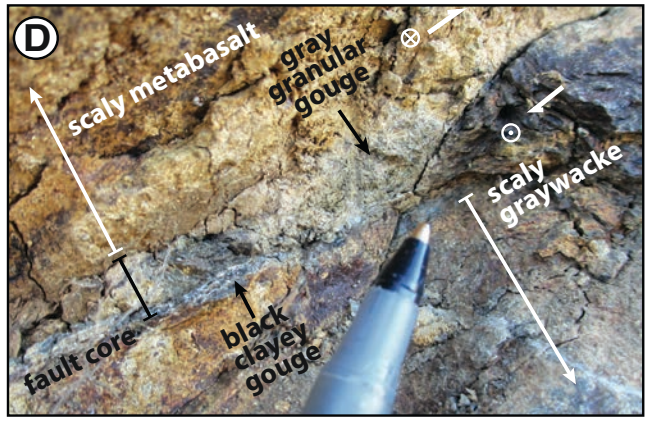
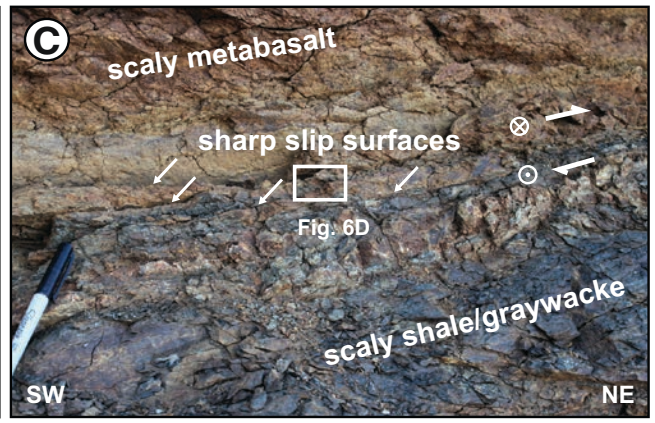
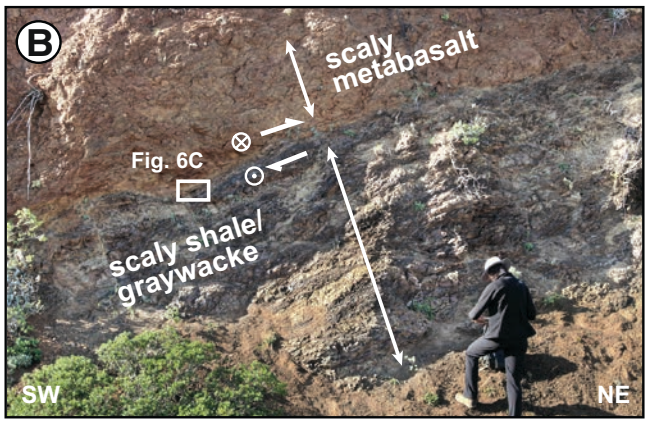
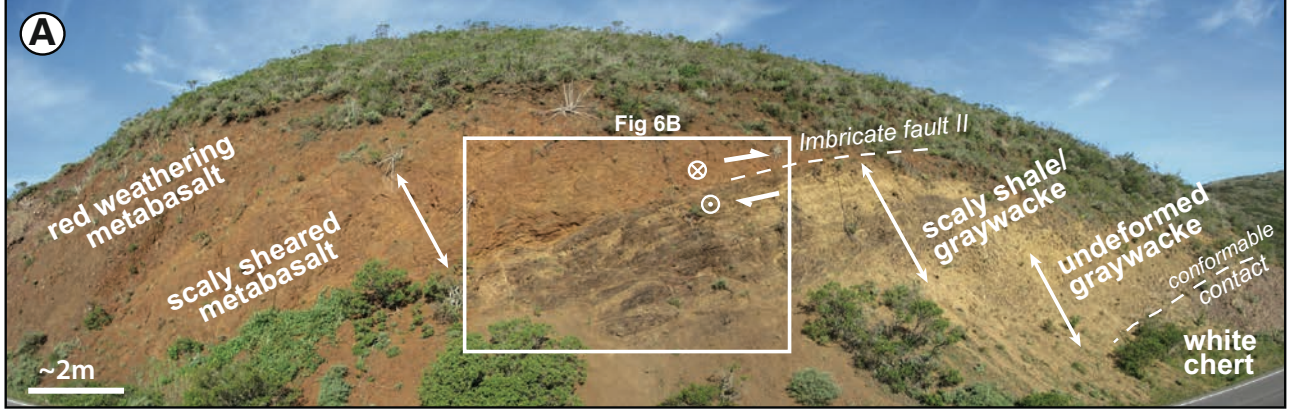
portion of the outcrop (Figs. 6C–6D). Downdip slickenlines on the principal slip surface are consistent with thrust motion on the fault. Below the fault core, there is an ~3.8-m-wide zone of scaly fabric that can be divided into two zones. The upper zone consists of ~2–3 m of relatively internally intact ~7–15 by 30–70 cm graywacke blocks in a dark black, metallic, clayey sheared matrix. Here, graywacke blocks occur as lenses bounded by an incipient, scaly shale fabric (Fig. 6E). The lower zone consists of ~1 m of scaly, anastomosing fabric in graywacke without a black sheared matrix. Graywacke blocks are ~10 cm by ~150 cm, lack an anastomosing fabric, and contain bedding-orthogonal fractures at ~5–10 cm spacing (e.g., Fig. 3F). This lower scaly unit has a relatively sharp lower contact with underlying graywackes. Undeformed graywacke in the footwall of the fault consists of gray, sandy lithic-dominated graywacke and minor interbeds of green-gray siltstone, with bedding-perpendicular fractures at >10–30 cm spacing (Fig. 6A). No veining was observed in either the scaly fabrics or within the fault core.

A second exposure of a metabasalt-over-graywacke imbricate-bounding thrust is visible ~300 m northeast of imbricate fault II (Figs. 2 and 6F–6G). Imbricate fault III has a similar overall architecture as imbricate fault II, but here, hanging wall and footwall lithologies are structurally mixed within a *mélange* zone, and there is no sharp planar principal slip surface in the fault core (Figs. 6F–6G). The total fault zone is an ~2.5-m-thick *mélange* that consists of four distinct units. The uppermost unit consists of ~50 cm of scaly fabric in metabasalt, with anastomosing fabric defining ~2–4-cm-thick by 10-cm-long phacoids, the asymmetry of which is consistent with the thrust sense of slip (*sensu* Moore, 1978). This unit has a sharp, wavy lower contact with an ~50-cm-wide unit of scaly fabric containing 20–50-cm-thick by 50–150-cm-long lenses of light-gray sandstone in a darker green-red matrix, likely derived from metabasalt (Fig. 6G). Fractured graywacke within these lenses has an incipient anastomosing or scaly fabric, with relatively more coherent lenses containing bedding-perpendicular fractures. Below this lithologically mixed unit, there is a second ~70-cm-wide horizon of monolithic scaly fabric in metabasalt with 2–10-cm-wide phacoids. This unit has a wavy lower contact with ~1.5 m of scaly fabric developed in graywacke, with an anastomosing fabric that defines ~20–50 cm phacoids. This unit has a sharp lower contact with underlying graywacke that is fractured parallel to bedding planes. There are no veins present in either the scaly fabrics or along any contacts between units.

### Styles of Folding in the Marin Headlands Terrane

The ribbon cherts in the Marin Headlands terrane are well known for spectacular examples of multiscale flexural slip folding, facilitated by the strong rheologic contrast between chert and shale beds in the ribbon chert section (Ellen, 1971; Wahrhaftig, 1984b). No folds have been observed in the other lithologies. Folds are disharmonic on scales of centimeters to meters, with straight limbs and smoothly curved to faulted hinges, most

**Imbricate Fault II**



**Imbricate Fault III**

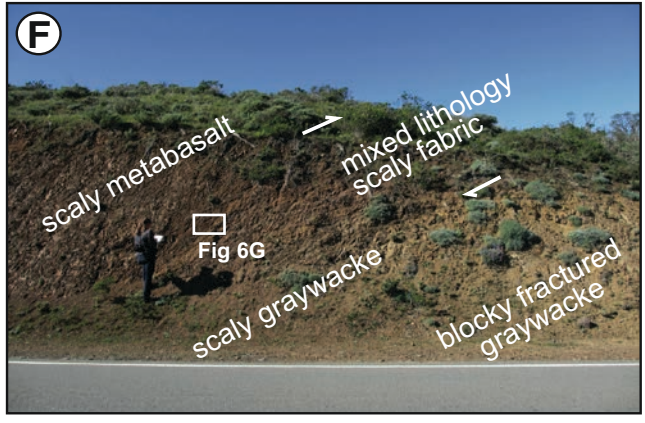


Figure 6. Field photographs of imbricate faults II and III. (A) Distorted panoramic of outcrop of imbricate fault II, showing thrust fault juxtaposing red-weathering metabasalt over trench sediments (interbedded graywacke and shale), which conformably overlie white chert. See Figure 2 for location. Box shows location of part B. (B) Slightly oblique roadcut through the sharp, discrete contact at imbricate fault II. Both hanging wall and footwall have a scaly shear fabric with elongation of fabric phacoids downdip. Box shows photo location of part C. (C) Close-up on the discrete, anastomosing sharp slip surfaces with black gouge layers that comprise the fault core of imbricate fault II. Sharp slip surfaces juxtapose bands of scaly gouge of different compositions. Box shows location of part D. (D) Photograph of the fault core of imbricate fault II. The upper contact of the fault core with scaly metabasalt and the lower contact with scaly shale/graywacke in the footwall are both sharp and planar. The fault core contains an ~0.5 cm upper granular gray gouge and an ~2-mm-thick lower, clayey gouge with phyllosilicates aligned in the direction of shear. (E) Lenticular interleaving of graywacke sandstone (yellow) and shale matrix (dark gray) in trench sediment units, in the footwall of imbricate fault II. (F) Imbricate fault III thrusts metabasalt (left) over graywacke (right). In contrast to imbricate fault II, this fault lacks a well-defined principal slip surface. Inset box shows location of part G. (G) Close-up of imbricate fault III showing a fractured lense of graywacke between lenses of scaly metabasalt. This tectonic interleaving defines the fault contact. Source lithologies in the tectonically interleaved portions of imbricate fault III are identifiable because they are preserved within relatively undeformed phacoids containing siliciclastic grains (graywacke) or mafic crystalline textures (metabasalt) that are visible in hand sample.

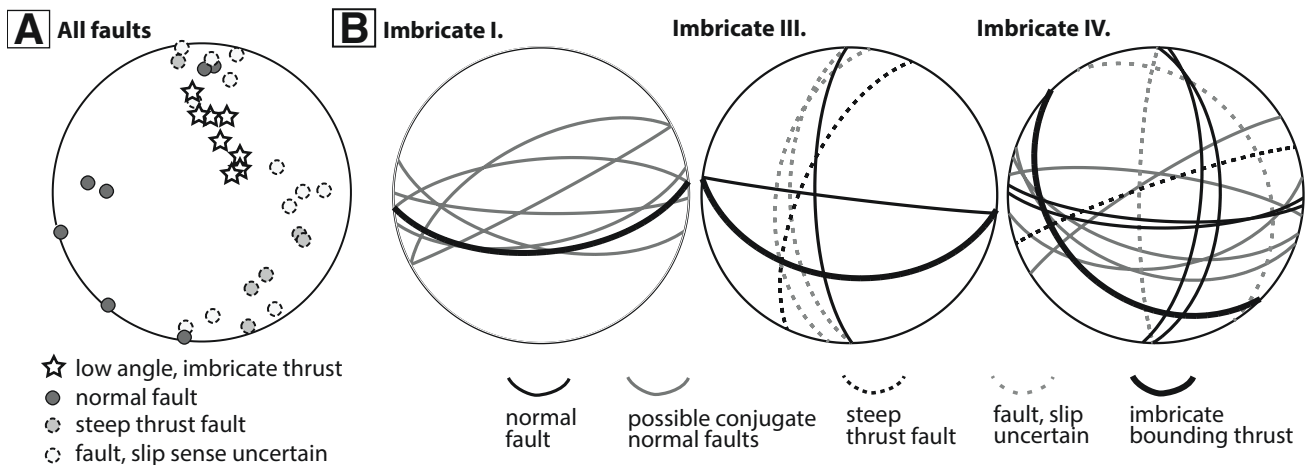


Figure 7. Structural data depicting styles of low- and high-angle faulting. (A) Comparison of all measured fault orientations, plotted as poles. Low-angle thrust faults cluster in a population that is distinct from populations of high-angle faults. The orientations of high-angle faults are quite variable, and there is overlap in the orientations of high-angle fault populations between each thrust sheet. High-angle faults do not have strikes similar to that of the modern San Andreas system (~330°–340°), and strike-slip slickensides were not observed. These data suggest that their formation was related to underthrusting or duplexing, rather than a late-stage overprint. (B) Orientations of high-angle faults within each imbricate sheet, sorted by slip sense. Each imbricate sheet has a unique set of high-angle faults, suggesting their formation was related to the variable stress state within each sheet during underthrusting or duplexing. Some of the minor, intraformational, E–W–striking normal faults have orientations consistent with that of conjugate sets with a steeply (~60°) SE-plunging  $\sigma_1$ , toward the paleotrench. These faults may be related to compaction during underthrusting. Other high-angle faults with apparent reverse, normal, or uncertain slip have large variability in orientation and often juxtapose different lithologic units. These faults may reflect accommodation of out-of-plane strain during underthrusting.

commonly forming chevron folds (Figs. 5A–5D). On average, folds in chert are asymmetric, with short, steep limbs on the north side, and longer, moderately dipping limbs on the south, suggesting north-vergence (Wahrhaftig, 1984a). However, we observed a wide variety in the styles, orientations, and scales of folding that can be used to identify faults dividing structural packages within lithologically homogeneous sections, for which we infer potentially significant offset.

Our data reveal significant variation in the strike and dip of axial planes and interlimb angles of folds in chert both within and between adjacent fault-bounded packages of sediment (Fig. 8).

High-angle faults that cut the entire exposed chert section (vertical extent of greater than tens of meters) are often associated with a change in fold style across the fault. Smaller-scale faults (lengths <10 m) contained within a single chert unit commonly crosscut and postdate folding. Gradual transitions from one fold domain to another are also observed over length scales of several meters. At one location, over an ~100 m strike-parallel distance, in the hanging wall of imbricate thrust IV, we observed open folds with inclined axial planes developed in near-vertical bedding, upright chevron folds with both planar and curved axial planes, asymmetric and symmetric chevron folds, and recumbent tight

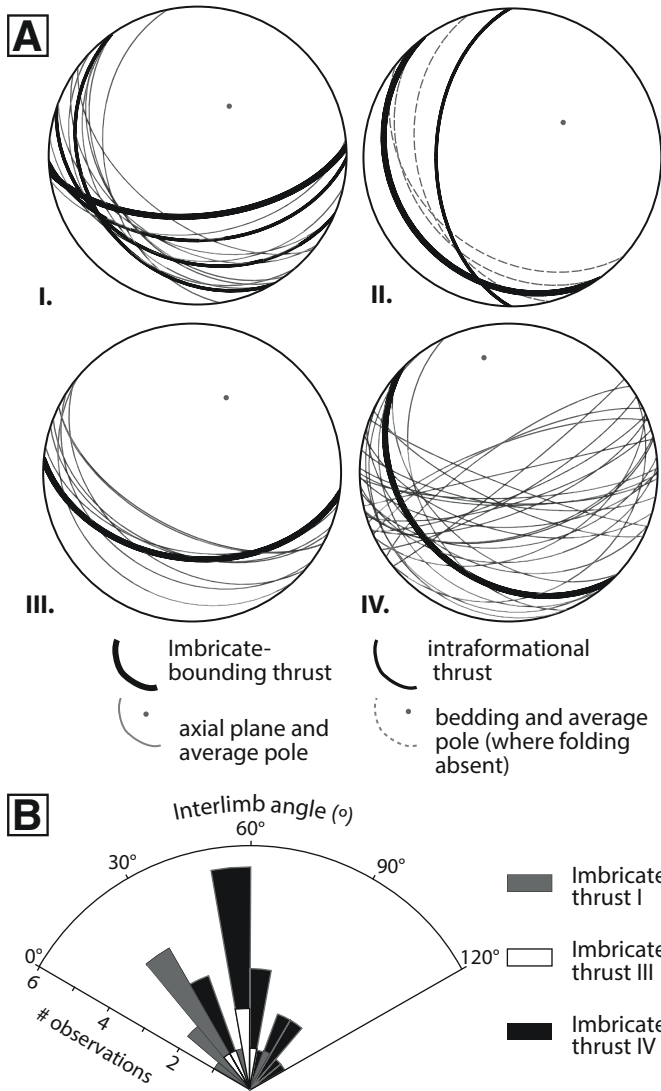


Figure 8. Structural data depicting variability in chert fold styles and vergence. (A) Stereonets showing the average orientations of axial planes within folded chert (thin lines), or average bedding where folding is absent (dashed lines) measured within the hanging wall of each major imbricate thrust, and the orientation of the bounding imbricate thrust fault (bold lines). Folds with each thrust sheet have a relatively unique set of fold axial plane orientations and indicate variation in vergence on the order of  $10^{\circ}$ – $40^{\circ}$  between adjacent imbricate sheets. (B) Rose diagram showing the interlimb angles of chert folds within each imbricate sheet.

folds (e.g., Fig. 5A). Such variations in fold style and interlimb angle may be explained by patchy variations in the maturity of diagenesis, and therefore in the effective viscosity, of the ribbon cherts during subduction (Murchey, 1984), or they may simply be a consequence of chaotic interlayer slip during folding. These lateral variations in fold chert rheology and fold style, however, may play a significant role in later localization of intrachert imbricate faults by disrupting the original planar stratigraphy.

Notable changes in fold vergence usually correspond to imbricate thrust faults (Figs. 2 and 8A). Average axial plane orientations display  $10^{\circ}$  to  $>40^{\circ}$  change in strike between adjacent thrust sheets (Fig. 8A). As average axial planes are usually subparallel to bounding thrust faults, we interpret the variation in fold vergence to reflect variation in thrust vergence between adjacent thrust sheets. We also observed variations in fold vergence within a single thrust sheet. For example, in imbricate sheet IV, there are multiple sets of axial planes with strikes that vary by  $20^{\circ}$ – $70^{\circ}$  (Figs. 5 and 8). Given that these folds are all contained in the hanging wall of a thrust that is not folded, we interpret the variation in axial plane orientation within a single thrust sheet to reflect that these cherts were not subject to plane strain during deformation, but rather experienced a component of shortening parallel to fault strike.

## DISCUSSION

### Conditions and History of Deformation in the Marin Headlands Terrane

We document three sets of structures corresponding to different expressions of strain: folding in the chert; steeply dipping, N-S- to NE-SW-striking faults; and moderately dipping, NNW-ESE-striking thrust faults (Fig. 9). Based on their orientation and vergence, we show that each of these groups of structures accommodated a different sense of strain. The meters-scale wavelength folds in the chert, which are predominantly N-verging, accommodated vertical thickening and N-S shortening (in today's coordinates). The steep, mostly normal or normal-oblique faults accommodated vertical thinning and approximately E-W elongation, and the thrust faults accommodated vertical thickening and roughly N-S shortening. As the Marin Headlands terrane has been rotated  $\sim 130^{\circ}$  clockwise since the time of accretion (Curry et al., 1984), the northward vergence and N-S shortening indicated by the folds in chert and the E-W-striking thrust faults would have originally been SW-vergent, consistent with the NE-directed subduction indicated by plate reconstructions for the latest Cretaceous (Stock and Molnar, 1988). The E-W extension suggested by the steep faults would have been oriented SE-NW, parallel to the Cretaceous margin. In the following sections, we discuss the conditions and relative sequence of deformation events indicated by our field observations.

### Initial Offscraping and Sediment Subduction

Graywackes imbricated in the Marin Headlands terrane originated as trench turbidites, and while their total original thickness is unknown, it is inferred that the uppermost section was offscraped and accreted at the toe of the wedge (Wahrhaftig, 1984a). The remaining sediment was subducted and, at least in part, imbricated and underplated at depth with the underlying chert and basalt. The thickness of the turbiditic graywacke in our mapped area is quite variable, and within a distance of a few kilometers, thickness ranges from  $\sim 5$  to  $\sim 100$  m. Some of this vari-

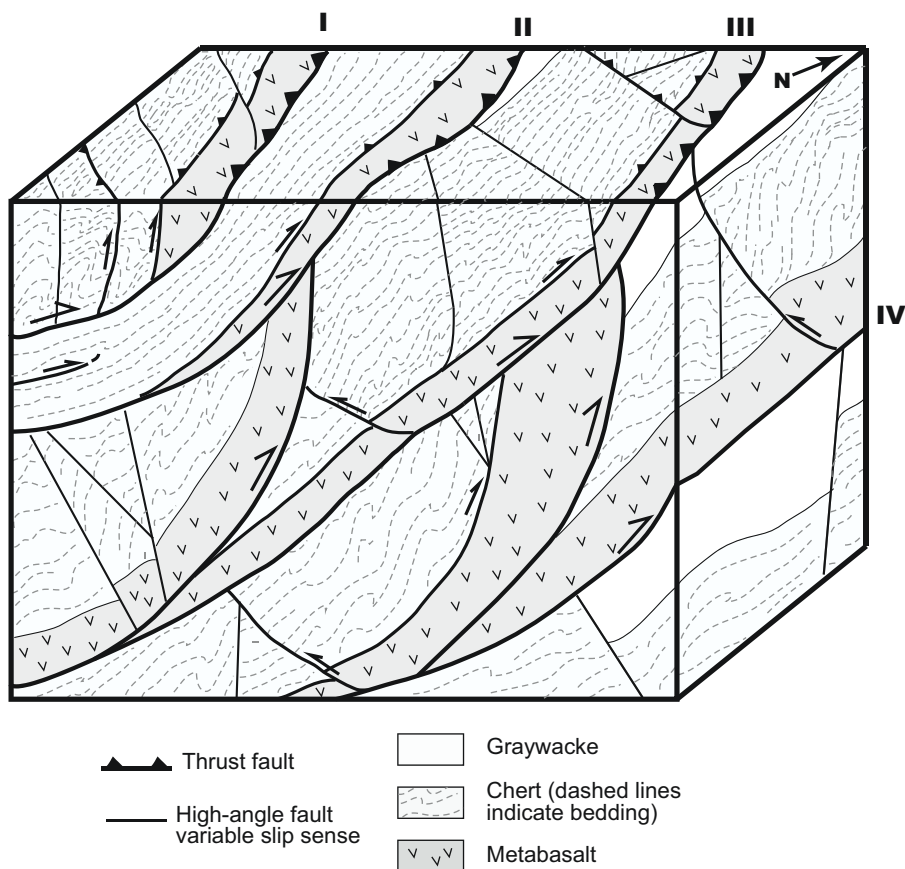


Figure 9. Schematic cartoon depicting our interpretation of the three-dimensional geometry of imbricate and high-angle fault systems in the Marin Headlands terrane. Major imbricate faults are labeled (see Fig. 2). See text for discussion.

ability may be due to initial clastic sediment thickness variations across distributary channel or fan systems in the Cenomanian trench or turbidity current scouring of sediments on the seafloor (Murchey, 1984; Wahrhaftig, 1984a). However, given the density of the faults we mapped along Conzelman Road, we consider it more likely that the true thickness is never preserved here and that the majority of thickness variations observed within the Marin Headlands terrane are rather the result of curvature of imbricate thrusts and of unmapped faults, which further deform the section. Lateral thickness variation in graywacke between thrust sheets may also be the result of variation in the stratigraphic level of the proto-décollement developed at the trench, which divided any offscraped trench units from the underplated units. Such a scenario can result from subduction of horst-and-graben topography and lateral variation in the thickness of downslope-transported sediment, as has been documented at the Japan Trench (Kodaira et al., 2012; Nakamura et al., 2013).

#### Deformation of Chert

Maroon-red ribbon cherts in the Marin Headlands terrane are pervasively folded, and bedding-normal white quartz veins are common, especially in the shale-rich sections. The hinges of the kink folds are often smoothly curved in individual thin beds (e.g., Fig. 5C), suggesting that the folds formed by ductile

deformation in the cherts and flexural slip along the chert/shale interlayers, at temperatures well below the onset of crystal plastic deformation in quartz. Bedding-normal quartz veins radiate around the hinges of folds, suggesting they formed before or during folding, consistent with deformation coinciding with early diagenetic compaction and dewatering. The kinematic similarity and the smooth transitions from thrust fault to fold axis (e.g., left side of Fig. 5B) suggest that, in general, the kink folds in chert formed simultaneously with similarly verging thrust faults. We therefore suggest that the onset of seaward-vergent fold and thrusting in the downgoing sediments occurred while the chert was not entirely lithified (cf. Kameda et al., 2012; Yamaguchi et al., 2016). Minor faults that crosscut folded cherts likely formed after chert lithification and transition to brittle behavior following the opal-CT to quartz transition (e.g., Kameda et al., 2012). As chert diagenesis is thought to be complete with transformation to quartz at  $\sim 80\text{--}150\text{ }^{\circ}\text{C}$  (Keller and Isaacs, 1985; Moore and Saffer, 2001), folding likely occurred at temperatures  $<150\text{ }^{\circ}\text{C}$ , corresponding to a depth of  $<15\text{ km}$  at a geothermal gradient of  $\sim 10\text{ }^{\circ}\text{C}/\text{km}$ , as estimated by Dumitru (1991) for the latest Cretaceous Franciscan forearc based on subducting plate age. At a typical subduction angle of  $\sim 14^{\circ}$  (Dumitru, 1991), the sediments would reach  $150\text{ }^{\circ}\text{C}$  at  $\sim 60\text{ km}$  landward of the trench. The differential shortening between folded chert horizons and

unfolded metabasalt was likely accommodated along the sheared lithologic chert-metabasalt contact observed at several locations on Conzelman Road (Fig. 2). The variation in fold style between fault-bounded blocks suggests that strain hardening due to chert folding may have helped localize intraformational faults.

### ***Development of Steeply Dipping Faults***

We identified 13 new, steeply dipping faults that juxtapose chert and metabasalt, or different subunits of chert (Figs. 2, 5, and 7). Most of the steeply dipping faults have true or apparent normal motion, as implied by flanking structures (usually bedding deflection or drag folds) and by foliation asymmetry and S/C fabrics (*sensu* Moore, 1978) and by ridge-and-groove lineations measured in the fault core. These faults cannot be traced over long distances, and they strike at a high angle to thrust faults that define the imbricate slices. We did not recognize any of these faults cutting clastic sediments, but this may be an artifact of the limited area of clastic sediments represented in our transect. In our transect, we observed no direct evidence of dextral shearing or any crosscutting relations that would imply that strands of the Cenozoic San Andreas system offset the Mesozoic subduction-related structures, consistent with the interpretations of Wakabayashi (1992). We also eliminate the possibility that these are part of the extensional system of faults that facilitated the Late Cretaceous–Paleocene exhumation of the Franciscan complex (Platt, 1986; Ring and Brandon, 1994; Unruh et al., 2007), because the limited extents of the faults in strike and in dip indicate that they are confined by the imbricate thrusts and must have been active before or during thrusting. Faults of this generation of regional exhumation have been primarily identified along the Franciscan–Great Valley boundary (the Coast Range fault) and seem to have passively exhumed the bulk of the Franciscan complex (Unruh et al., 2007).

We recognize three possible origins for these high-angle faults:

First, these may be normal or normal-oblique faults that became active as the subducting plate approached the trench, as is observed in modern subduction zones due to plate flexure (e.g., Ranero et al., 2003; Nakamura et al., 2013). High-resolution mapping of normal fault distribution on the incoming Pacific plate in the Japan Trench has identified both minor-scale faults at ~100 m spacing that have very small throw (~20–50 m) that offset only the sedimentary section, and larger faults with hundreds of meters of throw that cut down into the basaltic crust (Boston et al., 2014). Both scales of faults have very limited along-strike continuity (Boston et al., 2014). The spacing, throw, and lack of continuity of these normal fault systems are similar to the high-angle faults we observed juxtaposing chert with chert or chert with metabasalt. While some of the observed faults may emanate from reactivation of horst and grabens on the incoming plate, several of the observed high-angle faults crosscut chert folds or separate chert with different fold domains, and therefore must postdate some underthrusting and chert folding.

Second, these high-angle faults could have been activated either by compaction or by plate flexure or unflexure during subduction of the section. Some of the high-angle faults cut across the distinctive kink folds in the ribbon chert section, so they must have been active during or after subduction-related shortening of the chert. These faults may have therefore accommodated changes in thickness of the sedimentary section as the loading changed during underplating. Previous studies in underplated rocks have described similar patterns of strain, where initial underthrusting results in rapid burial of pelagic and trench sediments, resulting in vertical, bedding-normal shortening and layer-parallel extension (*cf.* Fisher and Byrne, 1987; Kimura and Mukai, 1991).

Third, the steep faults may have slipped after underplating and incorporation to the accretionary wedge. Normal and strike-slip faults commonly develop in the outer wedge in response to tectonic stresses, dynamic adjustments of the taper angle, and changes in the geometry of the downgoing plate. For example, small-offset (<100 m) normal and strike-slip faults occur at moderate to high angles to the Nankai trench axis, which accommodated trench-normal shortening, as well as local perturbations associated with the subduction of basement highs (Kington, 2012). High-angle faults mapped in the Nankai prism are nearly impossible to detect in trench-normal seismic lines, but they are visible in the three-dimensional seismic volume (Kington, 2012). It is possible then that the steep faults documented in the Marin Headlands terrane may have been active in association with subduction of rough seafloor bathymetry (Kington, 2012; Dominguez et al., 2000; Wang and Bilek, 2011), such as the Point Bonita Seamount terrane, which is in fault contact with the Marin Headlands terrane to the southwest (Fig. 1).

### ***Deformation along Imbricate Bounding Thrusts***

Our mapping indicates there exists a variety of structural styles in imbricate faults in the Marin Headlands terrane. Previously described thrusts in the Marin Headlands terrane are thick: Wahrhaftig (1984a) described faults transitioning into several-hundred-meter-wide *mélange* zones consisting of mixed graywacke, chert, metabasalt (greenstone), and serpentinite, and Meneghini and Moore (2007) described the Rodeo Cove thrust, a distributed fault zone ~60 m wide, consisting of heavily veined, interleaved metabasalt and chert. However, all of the faults exposed along Conzelman Road occur as sharp, discrete, <5-m-wide fault zones with thin, relatively planar fault cores, with minor or no lithologic mixing.

Both imbricate faults II and III are 2–5-m-thick zones of fault-parallel scaly fabric developed in metabasalt and graywacke. Imbricate fault III lacks the thin, sharp fault core observed in imbricate fault II and instead contains a mixing of lithologies within a sheared, *mélange* zone (Fig. 6). The difference in structural style between these faults may be a function of variable lithology within the footwall graywacke. At imbricate fault II, the presence of a black, scaly, shale matrix in the footwall fabric and a thin black gouge layer along a principal slip surface could have been the result of fault localization along a clay-rich unit

in the clastic sediments. Localization of slip along a thin, sharp, clay-rich horizon has been observed in cores recovered from the Nankai Trough (Sakaguchi et al., 2011) and Japan Trench (Chester et al., 2013; Kirkpatrick et al., 2015). The lack of a clay-rich horizon in the footwall of imbricate fault III may have led to strain hardening that promoted delocalization of slip and lithologic interleaving of hanging wall and footwall units.

These two faults, and all the minor faults shown in Figure 2, starkly contrast to the distributed style of faulting documented in the Rodeo Cove thrust (Meneghini and Moore, 2007), which bounds the structurally highest unit in the Marin Headlands terrane on the northeast side of the edge of the Point Bonita Seamount (Fig. 1). The Rodeo Cove thrust consists of a massive veined zone over 60 m thick, and it lacks a well-localized fault core (Meneghini and Moore, 2007). The lack of veining around any of the faults on our transect suggests that at the time of underplating, fluid generation from compaction and sediment diagenesis, including smectite-illite transition and opal dehydration, had run to completion, and any fluids sourced from basalt dehydration were either minimal or did not generate local fluid overpressures. The rocks in the Rodeo Cove thrust are the same lithologies and ages as the rocks composing the imbricate slices exposed along Conzelman Road, so the difference in veining abundance cannot be explained by lithology. One possible explanation is that the vein-forming fluids in the Rodeo Cove thrust may not have been locally sourced, but rather that this larger fault, which is at or near the top of the imbricate package, may have been a conduit for fluids sourced from deeper parts of the plate boundary. Another possibility is that cyclic variations in fluid pressure and stress field thought to promote veining at the Rodeo Cove thrust (e.g., Meneghini and Moore, 2007) may not be characteristic of the entire underplating history in the Marin Headlands terrane. The style of thrusting at Rodeo Cove may have been influenced by its proximity to the Point Bonita Seamount, which has a trace-element geochemistry of oceanic-island basalts (OIBs) rather than MORBs (Shervais, 1989), as are found in the rest of the Marin Headlands terrane (Ghatak et al., 2012), and which is much less internally deformed, with well-preserved pillows, dikes, and sills. It is possible that veining of the Rodeo Cove thrust was sourced from seamount-derived fluids, and that the Rodeo Cove thrust is an older structure related to the shearing and accretion of the Point Bonita Seamount, just before subduction and imbrication of the Marin Headlands terrane.

### Magnitude of Shortening and Time Scales of Imbrication

The sedimentary section exposed in the Marin Headlands terrane has been significantly shortened by multiple modes that can be grouped into faulting along major imbricate bounding thrusts, faulting along intraformational thrusts, and folding of the sedimentary section. In the section along Conzelman Road, we mapped five thrusts that bound large thrust sheets and place metabasalt or chert atop graywacke or chert. Given a chert + graywacke sediment thickness of ~100–300 m (Murchey, 1984;

Wahrhaftig, 1984a), and an average fault dip of 10°–30°, this requires a minimum slip of 200–1700 m on any individual thrust and a minimum cumulative slip of ~2300–6900 m across the five thrusts in our 1.5 km transect alone.

Additional increments of intraformational shortening are evident within both chert and metabasalt units. First, based on eight line-length restorations at four sites, intense folding within the cherts requires up to ~25%–46% of shortening internal to the sedimentary section (similar to estimate of <50% by Wahrhaftig, 1984a). Second, many internally undeformed metabasalt sections are overlain by intensely folded cherts, and the metabasalt-chert contacts are pervasively sheared. These observations suggest that the chert-metasalt lithologic contact was sometimes a favored localized shear horizon during chert folding, and possibly during later stages of subduction. Third, bedding-parallel faults that imbricate maroon-red chert require at least 20–40 m of apparent separation. Fourth, faults duplicating the metabasalt juxtapose pillowed and massive sections of similar dip. While no direct stratigraphic controls exist for the metabasalt, juxtaposition of different volcanic facies implies tens to hundreds of meters of throw, with an upper limit of ~300 m, the maximum thickness of metabasalt observed in Marin Headlands terrane imbricate structures (Wahrhaftig, 1984a). In total, we mapped at least six intraformational thrusts that imbricate sediment or metabasalt sequences of ~20 m or greater thickness, which result in an additional component of shortening within the Marin Headlands terrane. Assuming slip on intraformational faults with dips of 10°–30°, we obtain a minimum of 200–700 m of additional cumulative fault slip. We therefore estimate a minimum total of 2.5–7.6 km of shortening (elongation = ~20%–40%) within our ~1.5 km of mapped dip section through the Marin Headlands terrane exposed on Conzelman Road due to thrust faulting, not including shortening within folded chert sections.

These shortening estimates can be combined with published convergence rates during Marin Headlands terrane accretion to estimate the time scales of imbrication. Given Cenomanian microfossils in imbricated graywackes, the accretion of the Marin Headlands terrane must postdate ca. 95 Ma (Blake et al., 1984; Wakabayashi, 1992). Estimates of the rate of mid- to Late Cretaceous Farallon-Pacific plate convergence rates range from ~5 cm/yr (Hagstrum and Murchey, 1993) to ~10 cm/yr (Rea and Duncan, 1986). Accretion of the terrane was likely complete before the doubling in convergence rate associated with the onset of the Laramide orogeny at ca. 80 Ma (Alvarez et al., 1980; Rea and Duncan, 1986). Therefore, we take 5–10 cm/yr as a reasonable estimate of the convergence rate during imbrication of the Marin Headlands terrane. Assuming these plate rates, the 0.2–1.7 km of displacement observed along individual thrusts in the Marin Headlands could occur in 20–340 k.y., and the total of 2.5–7.6 km of shortening over all mapped thrusts could occur in 0.25–1.5 m.y. These data indicate that, on average, new faults accommodating the plate-boundary slip could be generated every ~10–100 k.y. In the end-member possibility that only one fault was active at a time, this would also represent the duration of

activity that any of these thrusts was active as the dominant plate-boundary fault segment. The intraformational thrust and reverse faults may have been simultaneously active with roof and/or sole thrusts, forming a duplex, or they may represent plate-boundary faults that were active for shorter durations and accumulated less displacement.

## **IMPLICATIONS FOR THE EVOLUTION OF UNDERPLATED SYSTEMS**

Our detailed mapping in the Marin Headlands terrane reveals a finer-scale, more kinematically complicated style of duplexing than represented by classic two-dimensional sections (e.g., Silver et al., 1985; Bernstein-Taylor et al., 1992; Fig. 9). In particular, we observe the following elements of geometric and kinematic complexity in the Marin Headlands terrane: (1) Major imbricate thrust sheets each have a variable vergence direction, indicating out-of-plane slip (relative to a trench-normal cross section) during underplating. (2) Multiple horizons in the basaltic crust and overlying sediment section acted as décollements, such that there does not appear to be a strong lithologic control on décollement localization. (3) Imbrication occurred on short length scales, such that the horizontal spacing between imbricate thrusts is on the order of tens to hundreds of meters. (4) Pervasive high-angle normal faulting within imbricate packages indicates layer-parallel extension and/or subvertical shortening during underthrusting. (5) Major high-angle faults with both apparent normal and reverse displacement juxtapose multiple stratigraphic units, including folded red ribbon cherts, bleached and altered cherts, and metabasalt.

Other underplated terranes also show evidence for kinematic complexity, closely spaced faults, and synsubduction thrust and normal faulting, which potentially record similarly complex geometries. Multiple detachment horizons have been identified in the internal Ligurian units of the Northern Apennines and in the Kodiak complex of Alaska (Meneghini et al., 2009; Marroni et al., 2010), and comparably short length scales of imbrication and variations in thrust vergence are implied by mapped sections of the Franciscan complex at Pacheco Pass (Kimura et al., 1996). Features of particular note in the Marin Headlands terrane are the high-angle faults that juxtapose otherwise coherent chert and metabasalt units within imbricate sheets (Figs. 5E–5F and 7). The high-angle faults we document have both apparent normal and thrust displacement and accommodate tens to hundreds of meters of throw, but they do not clearly crosscut multiple imbricate sheets. While minor intraformational normal faults and fractures associated with compaction during underthrusting have been documented in other underplated sections (e.g., Hashimoto et al., 2002; Kameda et al., 2012), we are not aware of any similar large-offset, high-angle faults that juxtapose different units within imbricate sheets documented in other underplated terranes.

We also note the following observations that imply significant variability in the internal architecture and mechanics of the plate boundary in regions of active underplating. In particular,

we observe: (1) relatively localized deformation associated with imbricate bounding thrusts. The metabasalt-over-graywacke faults we document are either sharp, thin fault zones with thin or absent damage zones, or zones of lithologic mixing over the ~5–10 m scale (Fig. 6). This is in contrast to previously documented 60- to >100-m-wide mélangé zones and zones of lithologic interleaving associated with metabasalt-over-chert imbricate thrusts in the Marin Headlands terrane (Wahrhaftig, 1984a; Meneghini and Moore, 2007). This diversity in fault style may be comparable to variability in stratal disruption at imbricate fault contacts in the Ligurian and Kodiak complexes (Meneghini et al., 2009). These observations imply that, in subduction zones with active underplating, there is potential for the coexistence of young fault segments with highly localized slip and wide distributed shear or mélangé zones. (2) None of the fault zones we observed in the Marin Headlands terrane contains veining. The relatively narrow, vein-free fault exposures we document are in contrast to the highly veined fault zones previously documented at Rodeo Cove (Meneghini and Moore, 2007) and in other underplated complexes. Abundant syndeformation quartz and calcite veining has been widely reported in other underplated sections, including in the Shimanto complex (Hashimoto et al., 2002), Hanazono complex (Onishi et al., 2001), and in the Ligurian Apennines (Meneghini et al., 2009), that is, more similar to the Rodeo Cove thrust (Meneghini and Moore, 2007). The contrast between our observations and these previously studied faults could be explained by the longevity or maturity of the faults, where the imbricate structures of the Marin Headlands terrane did not grow sufficiently in length or displacement to access sources of advecting fluid, or they were active for too short of a duration to develop significant vein systems.

In general, the thrust stacks mapped in the Marin Headlands terrane are consistent with duplex structures, but this idealized geometry may be significantly complicated by coeval activity of normal and oblique faults that accommodated vertical shortening and trench-parallel strain in the forearc. The variable thickness of imbricate sheets and multiple vergence directions of chert folds suggest that internal deformation between thrusts may have played a major role in thickening and shortening the section before, during, and after underplating. One possible explanation for the geometric and kinematic complexity of the underplated sections in the Marin Headlands terrane may be that it formed in association with subduction over rough seafloor bathymetry. Subduction over seafloor bathymetry can induce variations in thrust vergence and variability in underplated sediment section thickness. Additionally, subducted seafloor bathymetry may be associated with faults that develop at a high angle to the subduction interface, and it may additionally influence the directivity of coseismic slip, inducing deformation to step down into otherwise relatively coherent units (e.g., Dominguez et al., 2000; Kodaira et al., 2012; Kington, 2012; Nakamura et al., 2013). In this case, the spacing of the inherited faults in the downgoing plate would set the tempo for imbricating faults to develop (e.g., Nakamura et al., 2013).

Collectively, our data in the Marin Headlands terrane highlight the potential for rapid and frequent reorganization of the plate-boundary interface and provide evidence for heterogeneity of deformation within underplated sections over short length scales. Data from the Marin Headlands terrane imply that underplated terranes may record rapid rejuvenation of the plate-boundary thrust at 10–100 k.y. time scales by formation of closely spaced, relatively youthful faults with minimal displacement. At least in the shallow part of the subduction system (upper 10–15 km), imbrication and underplating act to refresh the active décollement surface, replacing maturing fault zones with fresh fractures through less-deformed rock. By preventing the maturation of faults by abandoning them before they accumulate sufficient slip, this process may affect the strength distribution of faults, the locking of the subduction thrust, and the accumulation of interseismic strain. The narrow faults and damage zones of the Marin Headlands terrane faults are generally consistent with limited cumulative displacement on each fault (e.g., Savage and Brodsky, 2010). The close spacing and compositional diversity of the faults in the Marin Headlands terrane would have led to variability in mechanical and rheological properties that affected the way in which the accumulation and release of plate-boundary strain evolved over short spatial (kilometer scale or less) and temporal (tens to hundreds of thousands of years) scales within the underplated system.

Our observations from the Marin Headlands terrane suggest that the small length scales of deformation and prevalence of out-of-plane strain may be common in underplated systems, but it may not be easily recognized in regions of poor outcrop exposure or sections that lack key marker horizons. In such systems, the stratigraphic position and deformational styles of fault interfaces developed within underplated sections can be variable over short (order of 100 m or less) distances. Such length scales of deformation are below the typical resolution of seismic-reflection data sets at typical depths of active underplating. Structures that accommodate internal deformation of imbricate thrust systems and out-of-plane strain may not be visible on two-dimensional seismic-reflection lines, or they may appear as seismically chaotic sections (cf. Nakamura et al., 2013; Kington, 2012). We suggest that the fine-scale geometric and kinematic complexity and the large variability in imbricate fault architecture documented in the Marin Headlands terrane may serve as an example of the complex style of deformation expected in regions of active underplating. The Marin Headlands terrane may be particularly applicable to systems involving thin subducted sediment sections and subduction of rough seafloor topography. Collectively, these observations reiterate the need for cross-comparison of geophysical and field observations when evaluating the kinematic and mechanical processes associated with underplating.

## CONCLUSIONS

We have presented the results of new mapping of a 2.5 km section (1.5 km in dip direction) of the Marin Headlands terrane,

where spectacular outcrops have recently been exposed by road work. The imbricate thrust sheets of the Marin Headlands terrane preserve the three-dimensional structural complexity inherent in underplating duplexes that cannot be explained by simple plane strain. Imbricate-bounding thrusts are spaced 10s to 100s of meters apart, with major thrusts spaced ~300 m, which, when combined with paleoconvergence rates of 5–10 cm/yr, suggest generation of new fault surfaces on the 10–100 k.y. time scale. The observations of steep faults internal to the imbricate packages (mostly normal, with minor strike-slip), and the variations in fold vergence and shortening direction between packages demonstrate a trench-parallel component of deformation before and during imbrication and underplating. The geometric complexity may be attributable to the effects of topography on the subducting plate, particularly associated with flexure at the trench or unflexure beneath the accretionary wedge. The frequent development of new, immature faults, as well as repeated disruption of the plate-boundary geometry by offset on steep structures, may “refresh” the plate-boundary interface and prohibit the evolution to a mature fault zone (*sensu* Rowe et al., 2013) at underplating depths (here, 8–10 km).

## ACKNOWLEDGMENTS

We thank J.C. Moore, H. Schwartz, M. Wildgoose, and J. Wakabayashi for productive discussions about Franciscan complex geology and subduction history, and Eleanor Seery for assistance with X-ray diffraction data. We also thank Francesca Meneghini and one anonymous reviewer for comments that helped improve the quality of the manuscript. Field accommodation was generously provided by B.D. Rowe, and supplementary field photography was supplied by E.M. Rowe. Funding for this work came from the U.S. National Science Foundation Postdoctoral Fellowship grant EAR-1349586 (Regalla, Singh) and the Wares Faculty Scholarship at McGill University (Rowe, Harrichhausen, Tarling).

## REFERENCES CITED

- Alvarez, W., Kent, D.V., Silva, I.P., Schweickert, R.A., and Larson, R.A., 1980, Franciscan complex limestone deposited at 17° south paleolatitude: *Geological Society of America Bulletin*, v. 91, no. 8, p. 476–484, [https://doi.org/10.1130/0016-7606\(1980\)91<476:FCLDAS>2.0.CO;2](https://doi.org/10.1130/0016-7606(1980)91<476:FCLDAS>2.0.CO;2).
- Bernstein-Taylor, B.L., Kirchoff-Stein, K.S., Silver, E.A., Reed, D.L., and Mackay, M., 1992, Large-scale duplexes within the New Britain accretionary wedge: A possible example of accreted ophiolitic slivers: *Tectonics*, v. 11, no. 4, p. 732–752, <https://doi.org/10.1029/91TC02901>.
- Blake, M.C., Jr., Howell, D.G., and Jayko, A.S., 1984, Tectonostratigraphic terranes of the San Francisco Bay region, *in* Blake, M.C., Jr., ed., *Franciscan Geology of Northern California*: Los Angeles, California, Pacific Section, Society for Economic Paleontologists and Mineralogists (SEPM), Book 43, p. 5–22.
- Boston, B., Moore, G.F., Nakamura, Y., and Kodaira, S., 2014, Outer-rise normal fault development and influence on near-trench décollement propagation along the Japan Trench, off Tohoku: *Earth, Planets, and Space*, v. 66, no. 1, p. 135–17, <https://doi.org/10.1186/1880-5981-66-135>.
- Calvert, A.J., 2004, Seismic reflection imaging of two megathrust shear zones in the northern Cascadia subduction zone: *Nature*, v. 428, no. 6979, p. 163–167, <https://doi.org/10.1038/nature02372>.

*Styles of underplating in the Marin Headlands terrane, Franciscan complex, California*

- Chester, F.M., Rowe, C., Ujiie, K., Kirkpatrick, J., Regalla, C., Remitti, F., Moore, J.C., Toy, V., Wolfson-Schwehr, M., Bose, S., and Kameda, J., 2013, Structure and composition of the plate-boundary slip zone for the 2011 Tohoku-Oki earthquake: *Science*, v. 342, no. 6163, p. 1208–1211, <https://doi.org/10.1126/science.1243719>.
- Curry, F.B., Cox, A., and Engebretson, D.C., 1984, Paleomagnetism of Franciscan rocks in the Marin Headlands, *in* Blake, M.C., Jr., ed., *Franciscan Geology of Northern California*: Los Angeles, California, Pacific Section, Society for Economic Paleontologists and Mineralogists (SEPM), Book 43, p. 89–88.
- Dominguez, S., Malavieille, J., and Lallemand, S.E., 2000, Deformation of accretionary wedges in response to seamount subduction: Insights from sandbox experiments: *Tectonics*, v. 19, no. 1, p. 182–196, <https://doi.org/10.1029/1999TC900055>.
- Dumitru, T.A., 1991, Effects of subduction parameters on geothermal gradients in forearcs, with an application to Franciscan subduction in California: *Journal of Geophysical Research*, v. 96, no. B1, p. 621–641, <https://doi.org/10.1029/90JB01913>.
- Ellen, S.D., 1971, The Development of Folds in Layered Chert of the Franciscan Assemblage near San Francisco, California [Ph.D. thesis]: Stanford, California, Stanford University, 339 p.
- Fisher, D., and Byrne, T., 1987, Structural evolution of underthrust sediments, Kodiak Islands, Alaska: *Tectonics*, v. 6, no. 6, p. 775–793, <https://doi.org/10.1029/TC006i006p0775>.
- Ghatak, A., Basu, A.R., and Wakabayashi, J., 2012, Elemental mobility in subduction metamorphism: Insight from metamorphic rocks of the Franciscan complex and the Feather River ultramafic belt, California: *International Geology Review*, v. 54, no. 6, p. 654–685, <https://doi.org/10.1080/00206814.2011.567087>.
- Graymer, R.W., Moring, B.C., Saucedo, G.J., Wentworth, C.M., Brabb, E.E., and Knudsen, K.L., 2006, Geologic Map of the San Francisco Bay Region: U.S. Geological Survey Scientific Investigations Map 2918, scale 1:275,000, <pubs.usgs.gov/sim/2006/2918>.
- Hagstrum, J.T., and Murchey, B.L., 1993, Deposition of Franciscan complex cherts along the paleoequator and accretion to the American margin at tropical paleolatitudes: *Geological Society of America Bulletin*, v. 105, p. 766–778, [https://doi.org/10.1130/0016-7606\(1993\)105<0766:DOFCCA>2.3.CO;2](https://doi.org/10.1130/0016-7606(1993)105<0766:DOFCCA>2.3.CO;2).
- Hashimoto, Y., and Kimura, G., 1999, Underplating process from mélange formation to duplexing: Example from the Cretaceous Shimanto belt, Kii Peninsula, southwest Japan: *Tectonics*, v. 18, no. 1, p. 92–107, <https://doi.org/10.1029/1998TC900014>.
- Hashimoto, Y., Enjoji, M., Sakaguchi, A., and Kimura, G., 2002, *P-T* conditions of cataclastic deformation associated with underplating: An example from the Cretaceous Shimanto complex, Kii Peninsula, SW Japan: *Earth, Planets, and Space*, v. 54, no. 11, p. 1133–1138, <https://doi.org/10.1186/BF03353314>.
- Hyndman, R.D., Wang, K., and Yamano, M., 1995, Thermal constraints on the seismogenic portion of the southwestern Japan subduction thrust: *Journal of Geophysical Research—Solid Earth*, v. 100, no. B8, p. 15,373–15,392, <https://doi.org/10.1029/95JB00153>.
- Kameda, J., Hina, S., Kobayashi, K., Yamaguchi, A., Hamada, Y., Yamamoto, Y., Hamahashi, M., and Kimura, G., 2012, Silica diagenesis and its effect on interplate seismicity in cold subduction zones: *Earth and Planetary Science Letters*, v. 317–318, p. 136–144, <https://doi.org/10.1016/j.epsl.2011.11.041>.
- Karl, S.M., 1984, Sedimentologic, diagenetic, and geochemical analysis of Upper Mesozoic ribbon cherts from the Franciscan assemblage at the Marin Headlands, California, *in* Blake, M.C., Jr., ed., *Franciscan Geology of Northern California*: Los Angeles, California, Pacific Section, Society for Economic Paleontologists and Mineralogists (SEPM), Book 43, p. 71–88.
- Keller, M.A., and Isaacs, C.M., 1985, An evaluation of temperature scales for silica diagenesis in diatomaceous sequences including a new approach based on the Miocene Monterey Formation, California: *Geo-Marine Letters*, v. 5, p. 31–35, <https://doi.org/10.1007/BF02629794>.
- Kelsey, H.M., 1978, Earthflows in Franciscan mélange, Van Duzen River basin, California: *Geology*, v. 6, no. 6, p. 361–364, [https://doi.org/10.1130/0091-7613\(1978\)6<361:EIFMVD>2.0.CO;2](https://doi.org/10.1130/0091-7613(1978)6<361:EIFMVD>2.0.CO;2).
- Kimura, G., and Mukai, A., 1991, Underplated units in an accretionary complex: Mélange of the Shimanto belt of eastern Shikoku, southwest Japan: *Tectonics*, v. 10, no. 1, p. 31–50, <https://doi.org/10.1029/90TC00799>.
- Kimura, G., Rodzdestvenskiy, V.S., Okumura, K., Melnikov, O., and Okamura, M., 1992, Mode of mixture of oceanic fragments and terrigenous trench fill in an accretionary complex: Example from southern Sakhalin: *Tectonophysics*, v. 202, p. 361–374, [https://doi.org/10.1016/0040-1951\(92\)90120-U](https://doi.org/10.1016/0040-1951(92)90120-U).
- Kimura, G., Maruyama, S., Isozaki, Y., and Terabayashi, M., 1996, Well-preserved underplating structure of the jadeitized Franciscan complex, Pacheco Pass, California: *Geology*, v. 24, p. 75–78, [https://doi.org/10.1130/0091-7613\(1996\)024<0075:WPUSOT>2.3.CO;2](https://doi.org/10.1130/0091-7613(1996)024<0075:WPUSOT>2.3.CO;2).
- Kimura, H., Takeda, T., Obara, K., and Kasahara, K., 2010, Seismic evidence for active underplating below the megathrust earthquake zone in Japan: *Science*, v. 329, p. 210–212, <https://doi.org/10.1126/science.1187115>.
- Kington, J.D., IV, 2012, The Structure and Kinematics of the Nankai Trough Accretionary Prism, Japan [Ph.D. thesis]: Madison, Wisconsin, University of Wisconsin, 124 p.
- Kirkpatrick, J.D., Rowe, C.D., Ujiie, K., Moore, J.C., Regalla, C., Remitti, F., Toy, V., Wolfson-Schwehr, M., Kameda, J., Bose, S., and Chester, F.M., 2015, Structure and lithology of the Japan Trench subduction plate boundary fault: *Tectonics*, v. 34, p. 53–69, <https://doi.org/10.1002/2014TC003695>.
- Kodaira, S., No, T., Nakamura, Y., Fujiwara, T., Kaiho, Y., Miura, S., Takahashi, N., Kaneda, Y., and Taira, A., 2012, Coseismic fault rupture at the trench axis during the 2011 Tohoku-oki earthquake: *Nature Geoscience*, v. 5, no. 9, p. 646–650, <https://doi.org/10.1038/ngeo1547>.
- Marroni, M., Meneghini, F., and Pandolfi, L., 2010, Anatomy of the Ligure-Piemontese subduction system: Evidence from Late Cretaceous–middle Eocene convergent margin deposits in the Northern Apennines, Italy: *International Geology Review*, v. 52, no. 10–12, p. 1160–1192, <https://doi.org/10.1080/00206810903545493>.
- Meneghini, F., and Moore, J.C., 2007, Deformation and hydrofracture in a subduction thrust at seismogenic depths: The Rodeo Cove thrust zone, Marin Headlands, California: *Geological Society of America Bulletin*, v. 119, no. 1–2, p. 174–183, <https://doi.org/10.1130/B25807.1>.
- Meneghini, F., Marroni, M., Moore, J.C., Pandolfi, L., and Rowe, C.D., 2009, The processes of underthrusting and underplating in the geologic record: Structural diversity between the Franciscan complex (California), the Kodiak complex (Alaska) and the Internal Ligurian units (Italy): *Geological Journal*, v. 44, no. 2, p. 126–152, <https://doi.org/10.1002/gj.1144>.
- Moore, J.C., 1978, Orientation of underthrusting during latest Cretaceous and earliest Tertiary time, Kodiak Islands, Alaska: *Geology*, v. 6, no. 4, p. 209–213, [https://doi.org/10.1130/0091-7613\(1978\)6<209:OUDLC>2.0.CO;2](https://doi.org/10.1130/0091-7613(1978)6<209:OUDLC>2.0.CO;2).
- Moore, J.C., and Saffer, D., 2001, Updip limit of the seismogenic zone beneath the accretionary prism of southwest Japan: An effect of diagenetic to low-grade metamorphic processes and increasing effective stress: *Geology*, v. 29, p. 183–186, [https://doi.org/10.1130/0091-7613\(2001\)029<0183:ULOTSZ>2.0.CO;2](https://doi.org/10.1130/0091-7613(2001)029<0183:ULOTSZ>2.0.CO;2).
- Moore, J.C., Diebold, J., Fisher, M.A., Sample, J., Brocher, T., Talwani, M., Ewing, J., von Huene, R., Rowe, C., Stone, D., and Stevens, C., 1991, EDGE deep seismic reflection transect of the eastern Aleutian arc-trench layered lower crust reveals underplating and continental growth: *Geology*, v. 19, no. 5, p. 420–424, [https://doi.org/10.1130/0091-7613\(1991\)019<0420:EDSRTO>2.3.CO;2](https://doi.org/10.1130/0091-7613(1991)019<0420:EDSRTO>2.3.CO;2).
- Moore, J.C., Rowe, C.D., and Meneghini, F., 2007, How can accretionary prisms elucidate seismogenesis in subduction zones?, *in* Dixon, T., and Moore, J.C., eds., *The Seismogenic Zone of Subduction Thrust Faults*: New York, Columbia University Press, MARGINS Theoretical and Experimental Earth Science Series, Volume 2, p. 288–315, <https://doi.org/10.7312/dixo13866-010>.
- Murchey, B.L., 1984, Biostratigraphy and lithostratigraphy of the chert in the Franciscan complex, Marin Headlands, California, *in* Blake, M.C., Jr., ed., *Franciscan Geology of Northern California*: Los Angeles, California, Pacific Section, Society for Economic Paleontologists and Mineralogists (SEPM), Book 43, p. 51–70.
- Murchey, B.L., and Jones, D.L., 1984, Age and significance of chert in the Franciscan complex in the San Francisco Bay region, *in* Blake, M.C., Jr., ed., *Franciscan Geology of Northern California*: Los Angeles, California, Pacific Section, Society for Economic Paleontologists and Mineralogists (SEPM), Book 43, p. 23–30.
- Nakamura, Y., Kodaira, S., Miura, S., Regalla, C., and Takahashi, N., 2013, High-resolution seismic imaging in the Japan Trench axis area off Miyagi, northeastern Japan: *Geophysical Research Letters*, v. 40, p. 1713–1718, <https://doi.org/10.1002/grl.50364>.

- Oleskevich, D.A., Hyndman, R.D., and Wang, K., 1999, The updip and down-dip limits to great subduction earthquakes: Thermal and structural models of Cascadia, south Alaska, SW Japan, and Chile: *Journal of Geophysical Research—Solid Earth*, v. 104, no. B7, p. 14,965–14,991, <https://doi.org/10.1029/1999JB900060>.
- Onishi, C.T., Kimura, G., Hashimoto, Y., Ikehara-Ohmori, K., and Watanabe, T., 2001, Deformation history of tectonic mélange and its relationship to the underplating process and relative plate motion: An example from the deeply buried Shimanto belt, SW Japan: *Tectonics*, v. 20, no. 3, p. 376–393, <https://doi.org/10.1029/1999TC001154>.
- Platt, J.P., 1986, Dynamics of orogenic wedges and the uplift of high-pressure metamorphic rocks: *Geological Society of America Bulletin*, v. 97, p. 1037–1053, [https://doi.org/10.1130/0016-7606\(1986\)97<1037:DOOWAT>2.0.CO;2](https://doi.org/10.1130/0016-7606(1986)97<1037:DOOWAT>2.0.CO;2).
- Ranero, C.R., Morgan, J.P., McIntosh, K., and Reichert, C., 2003, Bending-related faulting and mantle serpentinization at the Middle America Trench: *Nature*, v. 425, no. 6956, p. 367–373, <https://doi.org/10.1038/nature01961>.
- Rea, D.K., and Duncan, R.A., 1986, North Pacific plate convergence: A quantitative record of the past 140 m.y.: *Geology*, v. 14, p. 373–376, [https://doi.org/10.1130/0091-7613\(1986\)14<373:NPPCAQ>2.0.CO;2](https://doi.org/10.1130/0091-7613(1986)14<373:NPPCAQ>2.0.CO;2).
- Ring, U., and Brandon, M.T., 1994, Kinematic data for the Coast Range fault and implications for exhumation of the Franciscan subduction complex: *Geology*, v. 22, p. 735–738, [https://doi.org/10.1130/0091-7613\(1994\)022<0735:KDFTCR>2.3.CO;2](https://doi.org/10.1130/0091-7613(1994)022<0735:KDFTCR>2.3.CO;2).
- Rowe, C.D., Moore, J.C., Remitti, F., and IODP Expedition 343/343T Scientists, 2013, The thickness of subduction plate boundary faults from the seafloor into the seismogenic zone: *Geology*, v. 41, p. 991–994, <https://doi.org/10.1130/G34556.1>.
- Sakaguchi, A., Chester, F., Curewitz, D., Fabbri, O., Goldsby, D., Kimura, G., Li, C.-F., Masaki, Y., Sreaton, E.J., Tsutsumi, A., Ujiie, K., and Yamaguchi, A., 2011, Seismic slip propagation to the updip end of plate boundary subduction interface faults: Vitritine reflectance geothermometry on Integrated Ocean Drilling Program NanTroSEIZE cores: *Geology*, v. 39, p. 395–398, <https://doi.org/10.1130/G31642.1>.
- Sample, J.C., and Fisher, D.M., 1986, Duplex accretion and underplating in an ancient accretionary complex, Kodiak Islands, Alaska: *Geology*, v. 14, no. 2, p. 160–163, [https://doi.org/10.1130/0091-7613\(1986\)14<160:DAAUIA>2.0.CO;2](https://doi.org/10.1130/0091-7613(1986)14<160:DAAUIA>2.0.CO;2).
- Savage, H.M., and Brodsky, E.E., 2010, Collateral damage: Evolution with displacement of fracture distribution and secondary fault strands in fault damage zones: *Journal of Geophysical Research*, v. 116, no. B3, B03405, <https://doi.org/10.1029/2010JB007665>.
- Shervais, J.V., 1989, Geochemistry of igneous rocks from the Marin Headlands, in Wahrhaftig, C., and Sloan, D., eds., *Geology of San Francisco and Vicinity: 28th International Geological Congress Field Trip Guidebook 105*: Washington, D.C., American Geophysical Union, p. 40–41.
- Silver, E.A., Ellis, M.J., Breen, N.A., and Shipley, T.H., 1985, Comments on the growth of accretionary wedges: *Geology*, v. 13, p. 6–9, [https://doi.org/10.1130/0091-7613\(1985\)13<6:COTGOA>2.0.CO;2](https://doi.org/10.1130/0091-7613(1985)13<6:COTGOA>2.0.CO;2).
- St. Clair, J., Holbrook, W.S., Van Avendonk, H.J.A., and Lizarralde, D., 2016, Along-strike structure of the Costa Rican convergent margin from seismic a refraction/reflection survey: Evidence for underplating beneath the inner forearc: *Geochemistry Geophysics Geosystems*, v. 17, p. 501–520, <https://doi.org/10.1002/2015GC006029>.
- Stock, J., and Molnar, P., 1988, Uncertainties and implications of the Late Cretaceous and Tertiary position of North America relative to the Farallon, Kula, and Pacific plates: *Tectonics*, v. 7, no. 6, p. 1339–1384, <https://doi.org/10.1029/TC007i006p01339>.
- Unruh, J.R., Dumitru, T.A., and Sawyer, T.L., 2007, Coupling of Early Tertiary extension in the Great Valley forearc basin with blueschist exhumation in the underlying Franciscan accretionary wedge at Mount Diablo, California: *Geological Society of America Bulletin*, v. 119, no. 11–12, p. 1347–1367, <https://doi.org/10.1130/B26057.1>.
- Wahrhaftig, C., 1984a, The structure of the Marin Headlands block, California: A progress report, in Blake, M.C., Jr., ed., *Franciscan Geology of Northern California*: Los Angeles, California, Pacific Section, Society for Economic Paleontologists and Mineralogists (SEPM), Book 43, p. 31–50.
- Wahrhaftig, C., 1984b, A Streetcar to Subduction and Other Plate Tectonic Trips by Public Transport in San Francisco (revised edition): Washington, D.C., American Geophysical Union, 81 p., <https://doi.org/10.1029/SP022>.
- Wakabayashi, J., 1992, Nappes, tectonics of oblique plate convergence, and metamorphic evolution related to 140 million years of continuous subduction, Franciscan complex, California: *The Journal of Geology*, v. 100, p. 19–40, <https://doi.org/10.1086/629569>.
- Wang, K., and Bilek, S.L., 2011, Do subducting seamounts generate or stop large earthquakes?: *Geology*, v. 39, no. 9, p. 819–822, <https://doi.org/10.1130/G31856.1>.
- Yamaguchi, A., Hina, S., Hamada, Y., Kameda, J., Hamahashi, M., Kuwatani, T., Shimizu, M., and Kimura, G., 2016, Source and sink of fluid in pelagic siliceous sediments along a cold subduction plate boundary: *Tectonophysics*, v. 686, p. 146–157, <https://doi.org/10.1016/j.tecto.2016.07.030>.

